


RESEARCH ARTICLE

High-resolution integrated calcareous plankton biostratigraphy and magnetostratigraphy at the Oligocene–Miocene transition in Southwestern Atlantic Ocean

Rocco Gennari¹  | Davide Persico¹ | Elena Turco¹ | Giuliana Villa¹ |
Silvia Maria Iaccarino¹ | Fabio Florindo² | Pontus C. Lurcock² |
Geise de Santana dos Anjos Zerfass³

¹Dipartimento di Scienze Chimiche, della Vita e della Sostenibilità Ambientale, Parco Area delle Scienze 11/A, Parma, Italy

²Istituto Nazionale di Geofisica e Vulcanologia (INGV), Rome, Italy

³PETROBRAS/CENPES/PDGeo/BPA, Rio de Janeiro, Brazil

Correspondence

Rocco Gennari, Dipartimento di Scienze Chimiche, della Vita e della Sostenibilità Ambientale, Parco Area delle Scienze 11/A, 43124 Parma, Italy.

Email: rocco.gennari@unito.it

Funding information

Petrobras (Petróleo Brasileiro S.A.)

Handling editor: B. Aguirre-Urreta

After the formalization of the base of the Miocene in the Lemme-Carrosio section (Italy) at the base of Subchron C6Cn.2n, the calcareous plankton biostratigraphy was refined in several open ocean Deep Sea Drilling Project/Ocean Drilling Program sites. However, high-resolution quantitative biostratigraphic studies, integrating planktonic foraminifera and calcareous nannofossils, are still lacking for the time interval spanning the Oligocene–Miocene transition. Here, we present a reinvestigation of Deep Sea Drilling Project Hole 516F (Rio Grande Rise) and 4 oil wells drilled by Petrobras Brasileiro SA in the Campos Basin (SW Atlantic Ocean). We identified 12 planktonic foraminiferal and 18 calcareous nannofossil bioevents that have been integrated with an updated magnetostratigraphy of Hole 516F allowing the correlation with the GPTS and the identification of the Oligocene/Miocene boundary (base of Subchron C6Cn.2n) between the Top of *Sphenolithus delphix* and the Base of common *Paragloborotalia kugleri*. Furthermore, our results give new insights on the reliability of major calcareous plankton events across the Oligocene–Miocene transition: (a) the *Sphenolithus ciperensis* Top, the *S. delphix* Base and Top, and the *Sphenolithus cometa* Base are reliable events at a global scale; (b) the Bases of *Globoquadrina dehiscens* and *Sphenolithus disbelemnus* > 4 µm are correlatable events only within the study sector of the SW Atlantic Ocean; and (c) the *Globoturbotalita ciperensis* Top, *Globoturbotalita angulituralis* Top, and *Sphenolithus procerus* Base are diachronous. Finally, previously unreported biostratigraphic data, such as the distribution range of *S. disbelemnus* < 4 µm and *Sphenolithus* cf. *S. pseudoheteromorphus*, the *Tenuitellinata praestainforthi* acme interval, and the Top of common *Globigerinoides primordius* were identified in the Campos Basin.

KEYWORDS

calcareous nannofossil, high-resolution biostratigraphy, integrated stratigraphy, magnetostratigraphy, Oligocene–Miocene boundary, planktonic foraminifera

1 | INTRODUCTION

The Global Stratotype Section and Point (GSSP) of the base of the Neogene was formally defined in the Lemme-Carrosio section, in Northern Italy, at the base of Subchron C6Cn.2n, at meter 35, and approximated by means of the calcareous nannofossil *Sphenolithus*

delphix and *Sphenolithus capricornutus* ranges (35 to 32 m and 40 to 35 m, respectively) and by the planktonic foraminifer *Paragloborotalia kugleri* base, which occurs 2 m above the boundary (Steininger, Aubry, Berggren, Beard, & Jeffords, 1997).

The integrated bio-magnetostratigraphic framework of the Lemme-Carrosio section paved the way for successive detailed studies. The identification of the events that characterize the Oligocene/Miocene boundary (O/Mb) was refined through high-resolution calcareous nannofossil biostratigraphic correlations between the Lemme-

Rocco Gennari's current affiliation: Dipartimento di Scienze della Terra, Via Valperga Caluso 35, 10125 Turin, Italy.

Carrosio section and the Deep Sea Drilling Project (DSDP) Site 522 (Southeast Atlantic Ocean) and Ocean Drilling Program (ODP) Site 929 (equatorial Atlantic; Shackleton, Hall, Raffi, Tauxe, & Zachos, 2000). These authors provided an astronomical age of 22.9 ± 0.1 Ma for the boundary, which replaced the poorly defined age of 23.8 Ma in the time scale of Berggren, Kent, Swisher, and Aubry (1995). Retuning of ODP Site 929 to the La2004 astronomical solution resulted in an age of 23.03 Ma for the base of the Miocene (Lourens, Hilgen, Shackleton, Wilson, 2004). The Oligocene–Miocene transition (OMT) was studied in detail at ODP Sites 1218 (equatorial Pacific; Pälike, Frazier, & Zachos, 2006); 1090 (Southern Ocean; Billups, Pälike, Channel, Zachos, & Shackleton, 2004); 926, 928, and 929 (equatorial Atlantic, Curry et al., 1995; Pearson & Chaisson, 1997; Backman & Raffi, 1997); and 1264 and 1265 (Liebrand et al., 2016) and DSDP Sites 563 (Western North Atlantic, Miller et al., 1985; Maiorano & Monechi, 1998) and 516 (Berggren, Aubry, & Hamilton, 1983; Pujol, 1983; Spezzaferri, 1992, 1994; Wei & Wise, 1989). However, a high-resolution integrated calcareous plankton biostratigraphy, acquired by quantitative analyses, was not provided.

The DSDP Hole 516F, drilled during Leg 72, is one of the few deep-sea successions recovering the OMT in the subtropical Southwestern Atlantic and providing a magnetostratigraphic record and abundant and well-preserved planktonic foraminiferal and calcareous nannofossil assemblages. The above-mentioned studies on the OMT in Hole 516F were based on low-resolution sampling and on semi-quantitative biostratigraphic analyses, except for the study of Spezzaferri (1992) based on quantitative analysis on planktonic foraminifera. These studies produced different biostratigraphic and chronostratigraphic frameworks. Despite these differences, some of the planktonic foraminiferal data of Berggren et al. (1983) were incorporated into successive chronostratigraphic scales (Berggren, Kent, & van Couvering, 1985, 1995; Wade, Pearson, Berggren, & Pälike, 2011; Gradstein, Ogg, Schmitz, & Ogg, 2012) and the resulting bio-magnetostratigraphic age model was applied by several authors in paleoceanographic reconstructions across the OMT at Site 516 (e.g., Henderiks & Pagani, 2007; Pagani, Arthur, & Freeman, 2000; Plancq, Grossi, Henderiks, Simon, & Mattioli, 2012; Plancq, Mattioli, Henderiks, & Grossi, 2013).

The offshore subtropical Southwestern Atlantic Ocean is a strategic area for oil exploration (Mohriak, Mello, Dewey, & Maxwell, 1990) and was extensively drilled by Petrobras (Petrobras Brasileiro SA). Among the drilled oil wells, four (here named A, B, C, and D) were studied in this work, representing an opportunity to increase the amount of recovered sediments at the OMT. Abreu and Haddad (1998) previously investigated the Upper Eocene to Lower Miocene Well A by means of calcareous nannofossils, obtaining a low-resolution biostratigraphic framework across the OMT.

Here, we present: (a) a reexamination, at higher resolution and by means of quantitative analyses, of the calcareous plankton assemblages of Hole 516F, integrated with a new paleomagnetic study (this paper and Florindo et al., 2015) and (b) the results of a high-resolution calcareous plankton quantitative biostratigraphic study from the four Petrobras wells. Through the stratigraphic correlation of these successions, we aim to establish an up-to-date high-resolution bio-magnetostratigraphy of the OMT interval for the subtropical

Southwestern Atlantic and to give a contribution to the ongoing discussion on the taxonomy and biochronology of the calcareous plankton marker species of this stratigraphic interval.

2 | MATERIAL

We investigated the OMT interval in Southwestern Atlantic in DSDP Hole 516F and at four wells drilled by Petrobras (Petrobras Brasileiro SA; Figure 1). DSDP Hole 516F was cored on the northern flank of the Rio Grande Rise (Barker et al., 1983) at a water depth of 1,313 mbsl. Continuous coring operations started from 169.1 m subbottom and ended at 1,270.6 mbsf, slightly above the basaltic basement. The investigated interval spans from Core 3 (188.18 mbsf) to Core 11 (266.94 mbsf) and is characterized by two lithostratigraphic units. Unit 1 (188.18–193 mbsf) consists of poorly consolidated nannofossil ooze deposited above the lysocline and CCD, whereas Unit 2 (193–266.94 mbsf) consists of nannofossil and foraminiferal chinks with chert nodules and biogenic silica.

The four oil wells were cored in the Campos Basin (Figure 1), on the slope east of Cabo Frio (Brazil), at a water depth of approximately 1,000 mbsl, and they are here named Wells A, B, C, and D. Well A (2633.32–2673.05 m) shows a cyclic pattern made up of alternations of dark and light grey marls, with an overall mean thickness of 40 cm per cycle. In Well B (2944.22–2952.32 m), the cyclical pattern is less evident and made up of alternating clays and marls. Well C (2689.90–2754.77 m), similar to Well A, is composed of dark and light grey marl alternation, but from 2,730 m upward is characterized by the intercalation of several sandy layers that show a thickness reduction towards the top of the investigated interval. Well D (2692.19–2713.53 m) consists of sandstone beds in the lowermost 3 m and of the cyclical alternation of dark and light grey marls from 2,714 m up to the top of the investigated interval.

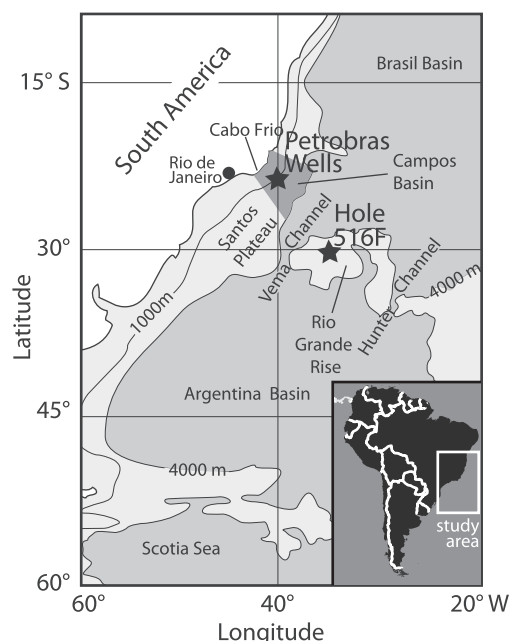


FIGURE 1 Location map of Wells A, B, C, and D in Campos Basin and of DSDP Hole 516F on the Rio Grande Rise

Five hundred and thirty-seven core samples were collected from Hole 516F (219 samples) and Wells A, B, C, and D (105, 37, 90, and 86 samples, respectively) with an overall average sampling distance of 28 cm; the almost continuous recovery of the studied cores allowed us to carry out a high-resolution quantitative biostratigraphy on the basis of planktonic foraminiferal and calcareous nannofossil assemblages.

One hundred thirty-nine samples were taken from Hole 516F between Core 3R-2 and Core11R-2 (189.72–266.7 mbsf), in order to obtain a high-resolution magnetostratigraphic record.

3 | METHODS

3.1 | Planktonic foraminifera

Core samples from Hole 516F and Wells A, B, C, D were heated in an electric oven at 40 °C for approximately 2 days to obtain dry samples and to measure their dry weight. Samples were processed with distilled water (Hole 516F) or H₂O₂ (3%; Wells A, B, C, and D) and washed with a 63- μ m sieve. Quantitative analyses of planktonic foraminiferal

assemblages were performed on splits of the >125 μ m fraction, containing approximately 200–300 individuals, obtained by using a microsplitter. Planktonic foraminiferal specimens were picked and fixed on Chapman slides and classified at a specific level, generic level, or as groups of species. The relative abundances of biostratigraphic markers (expressed as % of the total planktonic foraminiferal assemblage, see Data S1) were plotted for all the studied successions (Figures 2–6). Their quantitative distribution patterns allowed us to better pinpoint the events that define the (sub)zonal boundaries and to identify additional faunal changes (such as remarkable abundance variations and acme/paracme intervals), which may have a biostratigraphic significance, increasing the biostratigraphic resolution. The biostratigraphic scheme for tropical and subtropical regions of Wade et al. (2011) and Gradstein et al. (2012) and their astronomical recalibration of the bioevents were adopted.

3.2 | Calcareous nannofossils

All samples were prepared using the settling technique described by de Kaenel and Villa (1996) that assures a uniform and homogeneous distribution of nannofossils. Calcareous nannofossils were examined

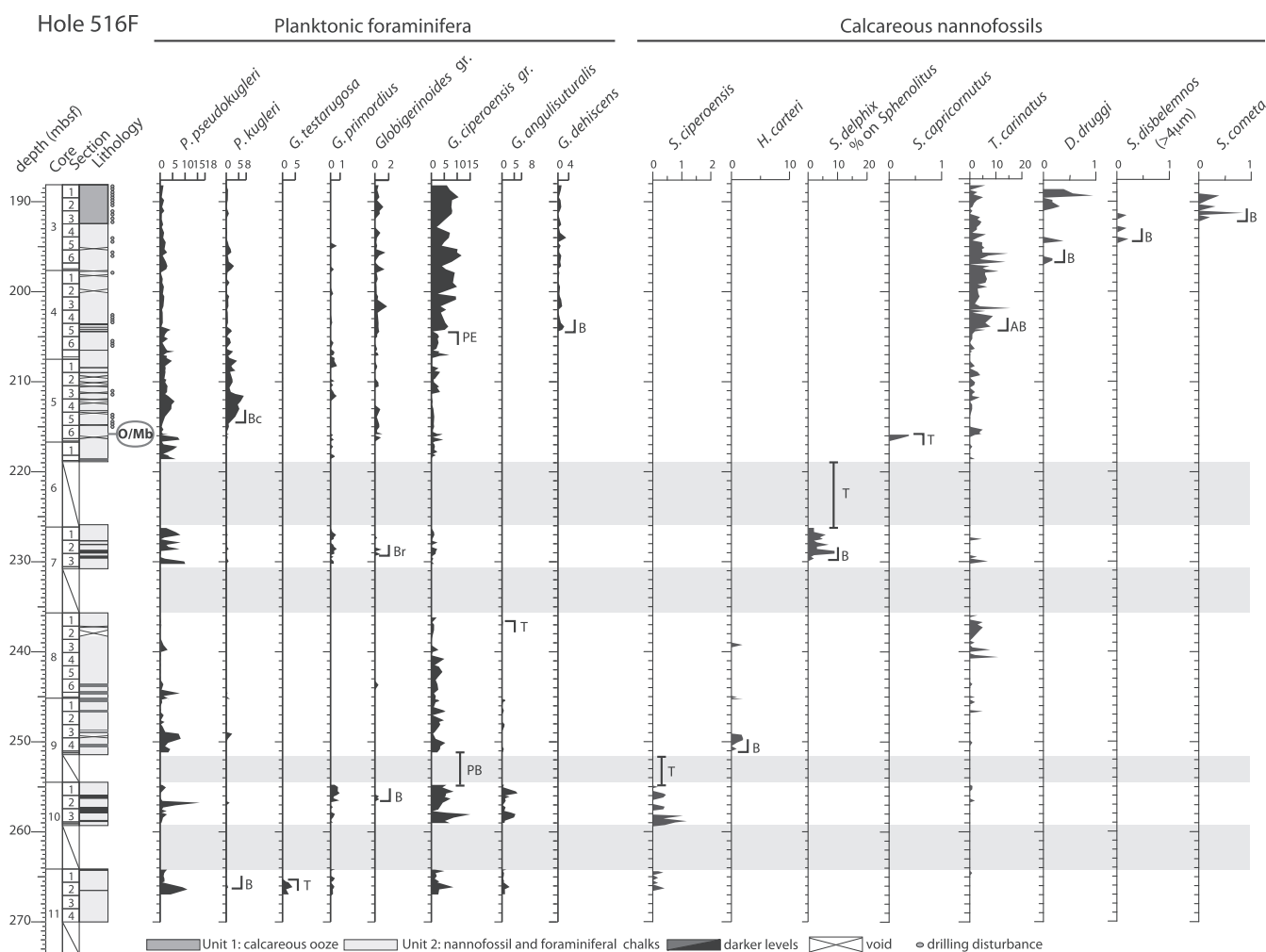


FIGURE 2 Plots of quantitative distribution pattern (%) of selected planktonic foraminifera and calcareous nannofossil taxa of Hole 516F. The grey boxes on the plots represent the no core recovery intervals and the grey circles besides the log indicate levels where drilling disturbance was detected. The Oligocene/Miocene boundary (O/Mb) is indicated with a grey circle beside the log. Note that the few Oligocene occurrences of *P. kugleri* correspond to the most prominent *P. pseudokugleri* abundance peaks

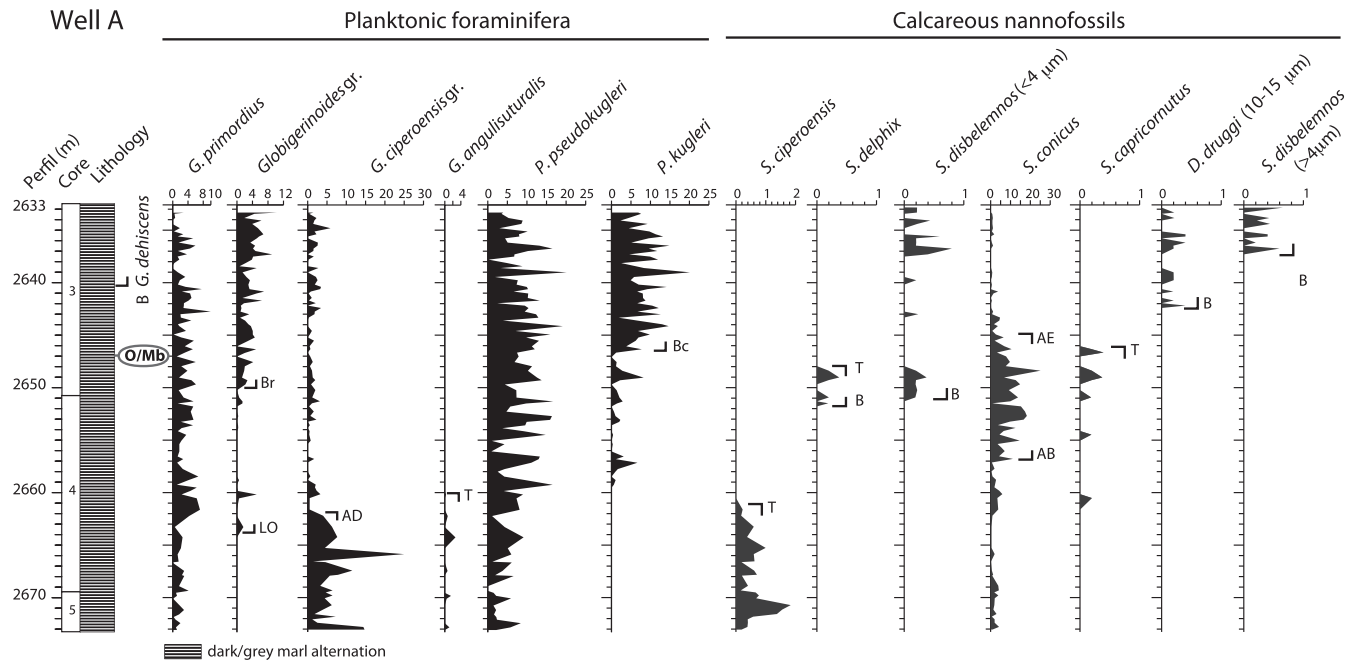


FIGURE 3 Plots of quantitative distribution patterns (%) of selected planktonic foraminifera and calcareous nannofossil taxa of Well A. Due to the paucity of *G. dehisces* throughout the well, its plot is not shown and the Base is indicated beside the lithologic log. The Oligocene/Miocene boundary (O/Mb) is indicated with a grey circle beside the log

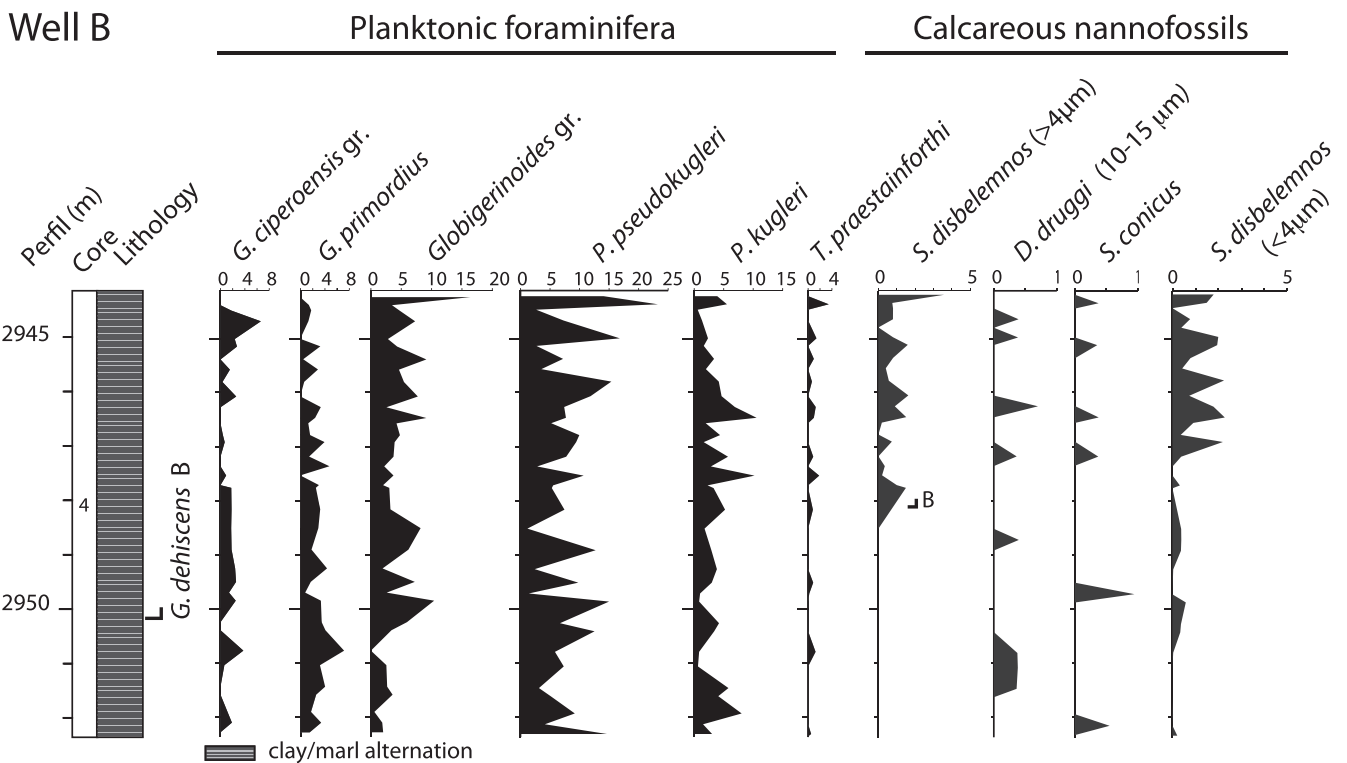


FIGURE 4 Plots of quantitative distribution patterns (%) of selected planktonic foraminifera and calcareous nannofossil taxa of Well B. Due to the paucity of *G. dehisces* throughout the well, its plot is not shown and the Base is indicated beside the lithologic log

under crossed-polarized light and phase-contrast light at 1,250× magnification. Quantitative analyses were performed by counting at least 500 specimens on each slide; two long traverses (200 fields of view) were scanned to detect specimens of rare taxa excluded from the initial counts. The conversion of the abundances to percentages and their

plots against depth allowed a detailed evaluation of the biostratigraphic events (Figures 2–6). The genus *Sphenolithus*, quite abundant in the Campos Basin wells, is conversely scarce in DSDP Hole 516F; thus, in the latter site, a supplementary counting regarding the index species versus a fixed number of *Sphenolithus* spp. was performed to

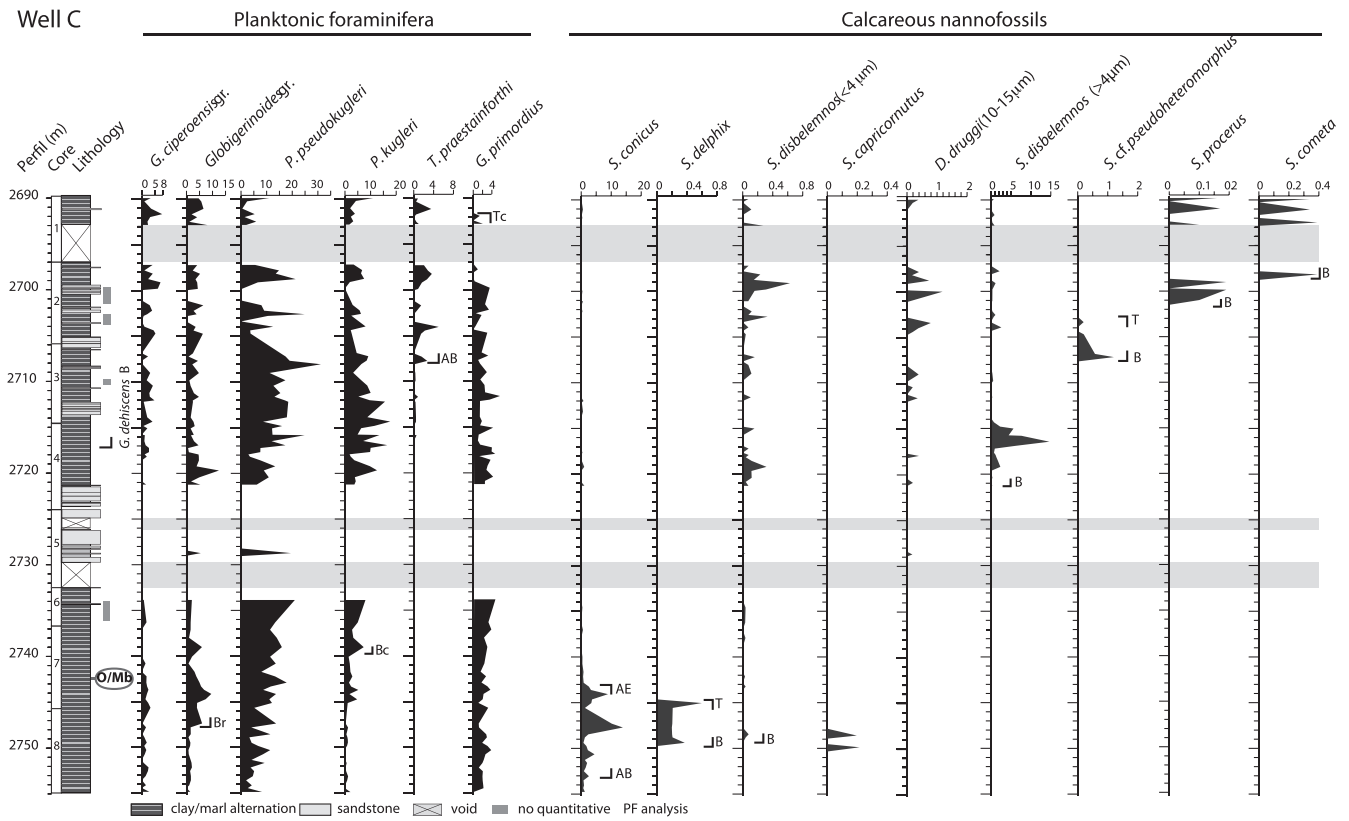


FIGURE 5 Plots of quantitative distribution patterns (%) of selected planktonic foraminifera and calcareous nannofossil taxa of Well C. Due to the paucity of *G. dehiscens* throughout the well, its plot is not shown and the Base is indicated beside the lithologic log. The grey boxes next to the lithologic log indicate intervals where quantitative analyses of planktonic foraminifers were hindered by the abundant terrigenous component present in the residues. The grey boxes on the plots represent the no core recovery intervals. The Oligocene/Miocene boundary (O/Mb) is indicated with a grey circle beside the log

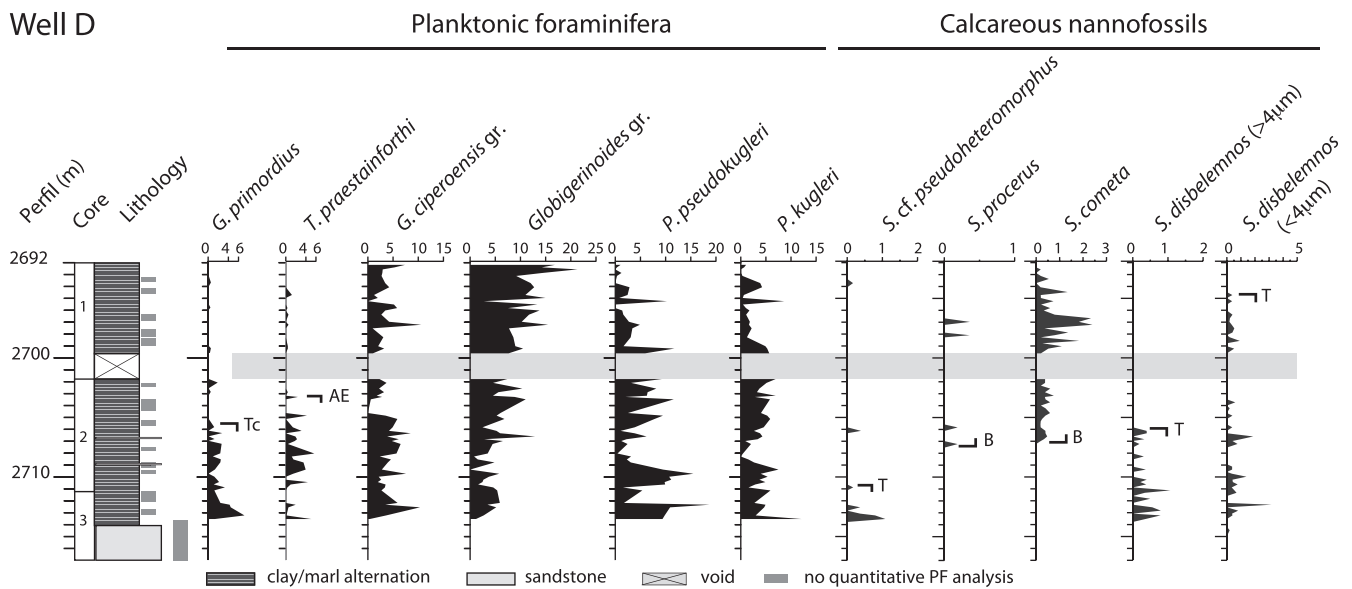


FIGURE 6 Plots of quantitative distribution patterns (%) of selected planktonic foraminifera and calcareous nannofossil taxa of Well D. The grey boxes beside the lithologic log indicate intervals where quantitative analyses of planktonic foraminifers were hindered by the abundant terrigenous component present in the residues. The grey boxes on the plots represent the no core recovery intervals

evaluate the distribution pattern of the marker species and compare them with their distribution in Campos Basin wells. The adopted biostratigraphic scheme for calcareous nannofossils is derived by an

integration of recently published biozonal schemes (e.g., Agnini et al., 2014; Backman, Raffi, Rio, Fornaciari, & Pälke, 2012) and the standard zonations of Martini and Farinacci (1971) and Okada and Bukry (1980).

3.3 | Paleomagnetism

DSDP Hole 516F was sampled using standard ~8 cm³ plastic cubes at the Integrated Ocean Drilling Program (IODP) Bremen Core Repository. Samples were oriented only with respect to the vertical; the geocentric axial dipole field at the latitude of the coring site has an inclination of ±49.4°, which makes it feasible to reconstruct paleomagnetic polarity using only inclinations.

To minimize sample dehydration and alteration, samples were packed in sealed bags and were stored in a refrigerated room until they were processed at the Istituto Nazionale di Geofisica e Vulcanologia, Rome. Natural and artificial magnetizations were measured at room temperature using a narrow-access pass-through 2-G Enterprises cryogenic magnetometer housed in a Lodestar Magnetics shielded room. After measurement of the natural remanent magnetization (NRM), samples were demagnetized in alternating field (AF) at successive peak fields of 5, 10, 15, 20, 25, 30, 35, 40, 45, 50, 60, 70, 80, and 100 mT. NRM stability was assessed using vector component diagrams (Zijderveld, 1967). Principal component analysis (Kirschvink, 1980) was used to calculate characteristic remanent magnetization (ChRM) directions, with linear best fits calculated from a minimum of three demagnetization steps using the PuffinPlot paleomagnetic analysis application (Lurcock & Wilson, 2012).

Following AF demagnetization of the NRM, a set of rock magnetic analyses was conducted on the same cube samples and on a selection of powder samples to investigate the magnetic mineralogy and to check its homogeneity throughout the core (Florindo et al., 2015).

4 | RESULTS

4.1 | Planktonic foraminifera

Preservation of planktonic foraminiferal assemblages varies from good, in Hole 516F, to moderate and poor, in Wells A to D. The poor preservation is the result of both fragmentation and recrystallization of the test wall, often hiding the original wall texture; this affected taxonomic assignment, as the wall structure is a discriminating character at generic level. Moreover, in the assemblages of Campos Basin wells, a variable but often large percentage of specimens (at times exceeding 60%) are small sized, not recognizable at specific/generic level. In Hole 516F, small-sized planktonic foraminifera are present as well but rarely exceed 30% of the total assemblage.

We identified 12 bioevents, indicated as Base (B) and Top (T), respectively, for the lowest and highest occurrences, Base common occurrence (Bc), Base regular occurrence (Br), Top common occurrence (Tc), Paracme Beginning (PB), Paracme End (PE), Acme Beginning (AB) and Acme End (AE; see Backman et al., 2012; Raffi et al., 2006). The recognized bioevents, labeled with increasing number in stratigraphic order in Table 1, are described and discussed below.

4.1.1 | Base and Base of common *Paragloborotalia kugleri*

Paragloborotalia kugleri, which evolves from *Paragloborotalia pseudokugleri* (following Blow, 1969), has a great stratigraphic importance at the OMT. In fact, the Base of *P. kugleri* defines the lower boundary of Zone M1 (Berggren et al., 1995; Wade et al., 2011) and

is used to approximate the O/Mb (Berggren et al., 1983, 1985, 1995; Steininger et al., 1997). In the Lemme-Carrosio section, the *P. kugleri* Base falls 2 m above the base of the Neogene, defined at the older end of Subchron C6Cn.2n (Steininger et al., 1997). This bioevent was astronomically dated at 22.96 Ma at Sites 925 and 926 (Lourens et al., 2004), in agreement with its magnetostratigraphic position in the Lemme-Carrosio section (Steininger et al., 1997), at Sites 522 (Shackleton et al., 2000) and 516 (Berggren et al., 1983), although, in the latter site, Subchron C6Cn.2n was not distinguished within Chron C6C. However, the Base of *P. kugleri* has been also associated with the youngest Oligocene Subchron C6Cn.2r at Site 1218 (equatorial Pacific; Lyle et al., 2002) and with Chron C7r (the reversal interval of Chron C7A in Spezzaferri, 1994) below the Top of the calcareous nannofossil *S. ciperoensis* (Berggren et al., 1983) in Hole 516F.

As noted by other authors (e.g., Keller, 1981; Pearson & Wade, 2009; Spezzaferri, 1991), the morphological transition between *P. pseudokugleri* and *P. kugleri* is gradual; thus, it is very important to have clear criteria to distinguish the two morphospecies. In Appendix A, we discuss in detail the taxonomy of the two species including the original description and subsequent modifications and we describe the taxonomic concepts adopted in this study.

The *P. pseudokugleri*-*P. kugleri* group is well represented in all the successions here investigated, although it is more abundant in the wells of Campos Basin than in Hole 516F. Within the studied assemblages, this group shows a gradual morphologic variability between the two end members, but we attempted to consistently separate them along the successions obtaining the quantitative distribution patterns of these two species (Figures 2–6).

Specimens (Figure 7(a), a1–a3) well comparable to *P. pseudokugleri* holotype of Blow (1969; Figure 7(b), a1–a3) are present with abundance fluctuations throughout the studied interval of Hole 516F and Wells A, B, C, and D. In Hole 516F, in correspondence of the levels of highest abundance of *P. pseudokugleri*, specimens showing the morphological features distinctive of *P. kugleri* (Figure 7(a), b–g) according to the original definition of Bolli (1957; Figure 7(b), b1–b3) are also recorded. These specimens closely resemble the *P. kugleri* individuals observed at its Base level in the Lemme-Carrosio section just above the O/Mb (Iaccarino, Borsetti, & Rogl, 1996), and those figured by other authors (e.g., Keller, 1981; Leckie, Farnham, & Schmidt, 1993; see Appendix A and Figure 7(b), d, f, and h). These forms discontinuously and rarely occur from Core 11 to Core 7 and become continuously present and relatively more abundant (>5%) from Core 5 upwards (Figure 2). On the basis of this distribution pattern in Hole 516F, very similar to that obtained in the same hole from a lower resolution sample set by Spezzaferri (1992), it is possible to distinguish the *P. kugleri* Base at 266.26 mbsf and its Base common at 214.28 mbsf (Figure 2).

A similar distribution pattern characterizes Well A (Figure 3), where *P. kugleri* is absent from the bottom of the investigated interval up to 2,659.99 m; above this stratigraphic level, *P. kugleri* shows irregular occurrences and becomes common (>5%) and continuously present above 2,646.49 m (Bc level). In Well C, this species is present and rare from the bottom to 2,740.38 m, where it shows an increase in abundance (with peaks >5%) and the Base of common *P. kugleri* is placed (Figure 5). In Well B (Figure 4), *P. kugleri* is continuously present

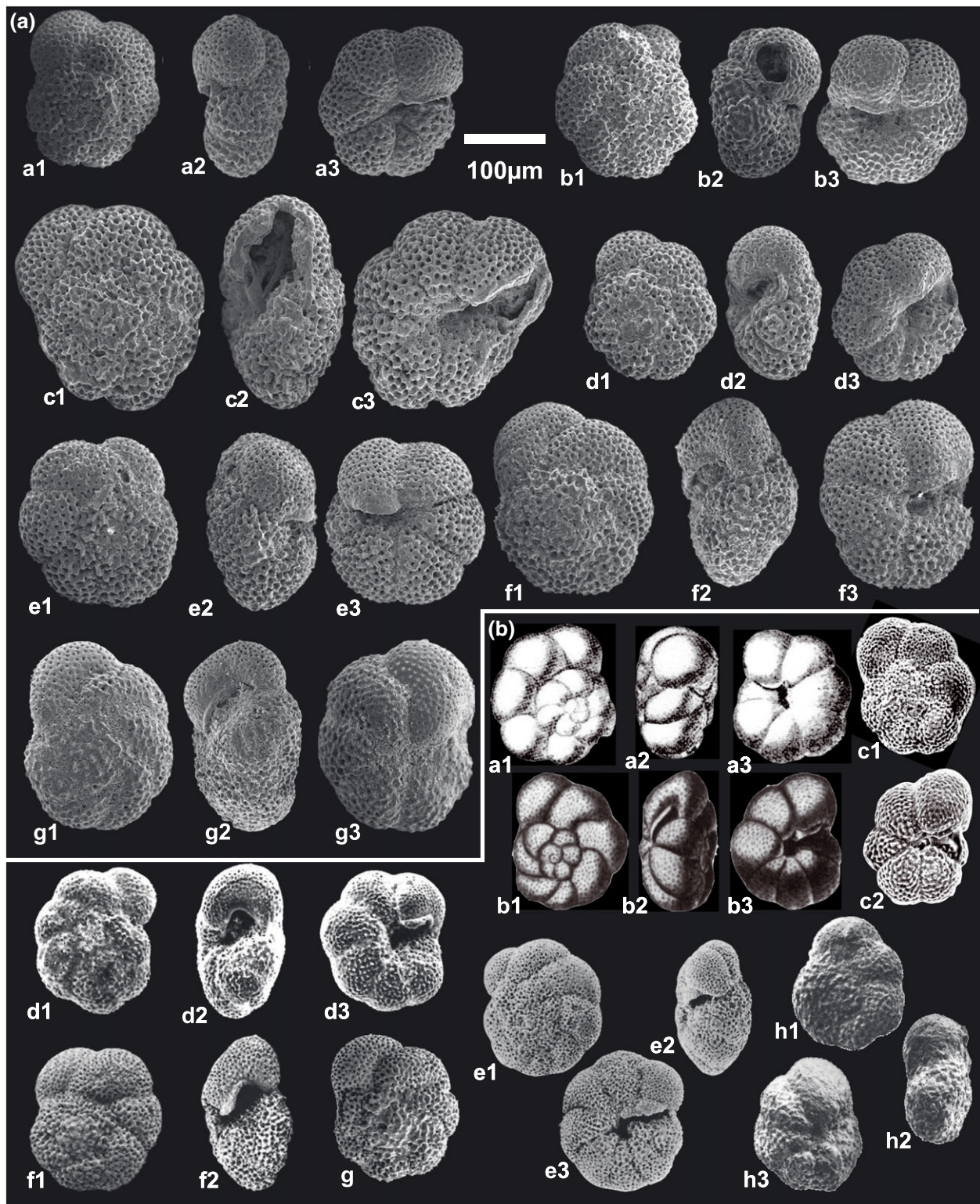


FIGURE 7 (a) *P. pseudokugleri* and *P. kugleri* specimens collected in Hole 516F (from progressively younger levels; this work): a1–a3, *P. pseudokugleri* (Sample 516F-11-2, 53–55 cm; 266.13 mbsf); b1–b3, *P. kugleri* (Sample 516F-11-2, 53–55 cm; 266.13 mbsf); c1–c3, *P. kugleri* (Sample 516F-9-3, 98.5–100.5 cm; 249.085 mbsf); d1–d3, *P. kugleri* (Sample 516F-8-7, 66–68 cm; 245.00 mbsf); e1–e3, *P. kugleri* (Sample 516F-7-3, 85–87 cm; 229.95 mbsf); f1–f3, *P. kugleri* (Sample 516F-5-5, 78–80 cm; 213.88 mbsf); g1–g3, *P. kugleri* (Sample 516F-5-4, 142–144 cm; 213.02 mbsf). (b) *P. kugleri* and *P. pseudokugleri* specimens as illustrated in previous works: a1–a3, *P. pseudokugleri* holotype (Blow, 1969); b1–b3, *P. kugleri* holotype (Bolli, 1957); c1–c2, *P. pseudokugleri* paratype (Blow, 1969); d1–d3, *P. kugleri* (292-17-6, from Keller, 1981); e1–e3, *P. kugleri* s.s. (Sample 709B-22-3, 80–85 cm, from Spezzaferri, 1991); f1–f2, *P. kugleri* (sample 803D-35X-5, 50–52 cm, from Leckie et al., 1993, picked in the base level of the species); g, *P. pseudokugleri* (Trinidad, Mosquito Creek, close to the type locality of Blow's, 1969 species, sample PP07/TT7; see Pearson & Wade, 2009), according to the authors this sample was collected in the Oligocene biozone O6 of Berggren & Pearson, 2005); h1–h3, *P. kugleri* (Lemme-Carrosio section, sample LE III-33, 2 m above the GSSP of the base of the Neogene, from Iaccarino et al. (1996) [Colour figure can be viewed at wileyonlinelibrary.com]

and commonly exceeds 5%, whereas in Well D (Figure 6), the continuous distribution is associated with lower abundances, generally <5%.

4.1.2 | Top of *Globorotaloides testarugosa*

According to Spezzaferri (1994), the Top of *G. testarugosa* is a reliable event only in the Southern Atlantic and Pacific Oceans, where it post-dates the Base of *P. kugleri*.

In our material, *G. testarugosa* (Figure 8, a1–a3) is present only in Hole 516F where its Top is recorded at 265.35 mbsf, postdating the Base of *P. kugleri* (Figure 2).

4.1.3 | Base and Base of common *Globigerinoides* group

The *Globigerinoides* event was defined by Spezzaferri (1994) as the Base of one of the following species: *Globigerinoides immaturus*, *G. quadrilobatus*, *G. parawoodi*, *G. bollii*, *G. subsacculifer*, and *Globigerinoides* cf. *G. subquadratus*. The author considered this event globally synchronous, taking place “in the first third of the total range distribution of *P. kugleri*.” Spezzaferri (1994) did not include *Globigerinoides trilobus* in this group, whose Base was observed at different levels in the early Miocene biozones N4 and N5, therefore

diachronous at a global scale. Differently, Pearson and Chaisson (1997) lumped *G. trilobus* with *G. immaturus* and observed their appearance at the base of the Miocene (at 22.96 Ma according to Lourens et al., 2004). In the Lemme-Carrosio section, the *Globigerinoides* gr. included all the species except “*G. primordius* (Iaccarino et al., 1996) and the Base of the group was observed in the late Oligocene, within Chron C6Cr and below the *P. kugleri* Base; at Lemme-Carrosio, the first species to appear is *G. parawoodi* (Spezzaferri, 1996), making this event equivalent to the “*Globigerinoides* event” of Spezzaferri (1994). In this study, we retain the *Globigerinoides* gr. definition of Iaccarino et al. (1996); see also Appendix A).

Overall, in Hole 516F (Figure 2), the *Globigerinoides* gr. (Figure 8, b and c) is rare and generally <2%, although it is more common in the Campos Basin wells (up to 21.32% in Well D). In Hole 516F, the Base of the *Globigerinoides* gr. (0.62%), represented by *Globigerinoides* cf. *G. subquadratus*, is recognized at 256.43 mbsf. This group is discontinuously present in the lower part of its range, whereas it becomes relatively more regularly distributed above 229.20 mbsf (Br). A similar distribution pattern of the *Globigerinoides* gr. is observed in Well A (Figure 3), where the Base, represented by *G. quadrilobatus* and *G. trilobus* s.l., is defined at 2,663.74 m, and the Base of regular

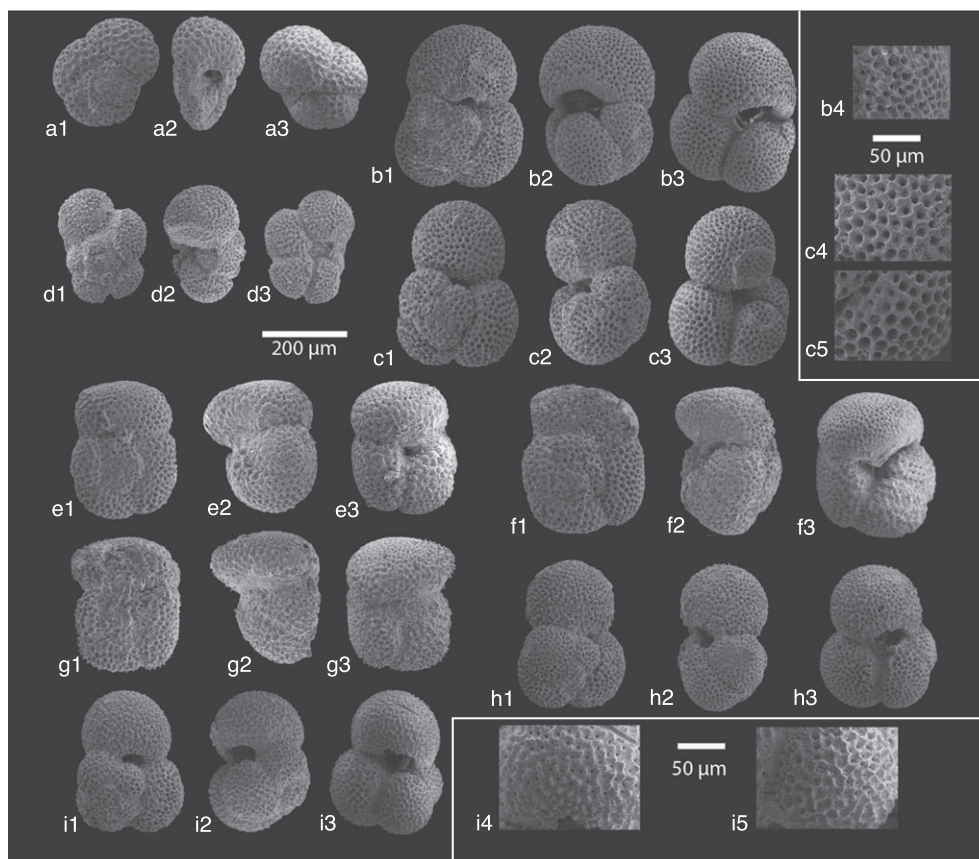


FIGURE 8 Planktonic foraminifera of hole 516F. 1 = spiral view, 2 = lateral view, and 3 = umbilical view: a1–a3, *Globorotaloides testarugosa* (Sample 516F-11-2, 53–55 cm; 266.13 mbsf); b1–b4, *Globigerinoides quadrilobatus* (Sample 516F-4-3, 102–104 cm; 201.62 mbsf); b4, detail of the last chamber; c1–c5, *Globigerinoides* sp. 1 (Sample 516F-3-7, 5–7 cm; 197.15 mbsf; see plate 15, fig. 4a–c, Spezzaferri (1994)); c4 and c5 details of the ultimate and penultimate chambers; d1–d3, *Globoturborotalita angulituralis* (Sample 516F-11-2, 53–55 cm; 266.13 mbsf); e1–e3, *Globoquadrina dehiscens* (Sample 516F-4-5, 63–65 cm; 204.23 mbsf); f1–f3, *Globoquadrina dehiscens* (Sample 516F-4-3, 102–104 cm; 201.62 mbsf); g1–g3, *Globoquadrina dehiscens* (Sample 516F-3-7, 5–7 cm; 197.15 mbsf); h1–h3, *Globigerinoides primordius* (Sample 516F-10-1, 137–139 cm; 255.97 mbsf); i1–i5, *Globigerinoides primordius* (Sample 516F-10-2, 45–47 cm; 256.55 mbsf); i4, wall texture magnification of the last chamber; i5, wall texture magnification of antepenultimate chamber

occurrence at 2,649.96 m (2.17%). In the other wells of the Campos Basin (Figures 4–6), the *Globigerinoides* gr. is present from the base of the studied intervals: In Well C, this group shows an abundance increase and a more continuous distribution from 2,747.51 m upwards (6%), where its Base of regular occurrence is placed, whereas in Wells B and D, it is common (quite regularly >5%) and continuous throughout the studied intervals.

4.1.4 | Paracme interval of *Globoturbotalita ciproensis* gr.

Within the *G. ciproensis* gr., we lumped together all the five-chambered *Globoturbotalita* species except for *G. angulisuturalis*, thus including *G. ciproensis*, *G. ciproensis fariasi*, *G. anguliofficialis*, and *G. ottangensis*. According to Pearson and Chaisson (1997), all these species are well represented in the Oligocene Atlantic low-latitude planktonic foraminiferal assemblages and disappear during the early Miocene. In particular, the Top of *G. ciproensis* in ODP Sites 925 and 926 is recorded near the O/Mb, successively calibrated at 22.90 Ma by Lourens et al. (2004; see also Wade et al., 2011).

The *G. ciproensis* gr. dominated by *G. ciproensis*, is present along all the studied successions, showing abundance fluctuations. In Hole 516F, this group is characterized by a paracme interval, where it shows abundances lower than 5%, from 252.97 to 204.32 mbsf (Figure 2). These stratigraphic levels are indicated as Paracme Beginning (PB) and Paracme End (PE), respectively; however, the exact position of the PB is obscured by an interval of no core recovery between 251.16 and 254.77 mbsf.

In Well A (Figure 3), the *G. ciproensis* gr. regularly exceeds abundances of 5% (with peaks >10%) from the base of the studied interval up to 2661.91 m; at this level, a remarkable abundance drop (AD) occurs and the group steadily shows abundances lower than 2% up to the top of the investigated interval, except for an abundance spike at approximately 2,634.5 m. Thus, in Well A, the paracme interval is replaced by a decrease in abundance. In Wells B and C, *G. ciproensis* gr. shows relative abundances generally lower than 5% except for a few peaks above 2,945 m in Well B and above 2,700 m in Well C; in both cases, it shows a poorly defined upward increasing trend (Figures 4 and 5). In the investigated interval of Well D, this group is always present with abundances ranging from 0.39% to 10.6% (Figure 6).

4.1.5 | Top of *Globoturbotalita angulisuturalis*

Globoturbotalita angulisuturalis is easily distinguishable from the *G. ciproensis* gr. by its characteristic U-shaped sutures (Figure 8, d1–d3). The Top of *G. angulisuturalis* occurs in the early Miocene and was calibrated at 20.94 Ma (Gradstein et al., 2012). This age calibration is based on the stratigraphic position of this event reported by Berggren et al. (1983) in Hole 516F. However, in the same hole, Pujol (1983) and Spezzaferri (1994) observed the same event at a much lower stratigraphic level, in the late Oligocene. A late Oligocene Top, a few meters above the Top of *S. ciproensis*, is also indicated by Pearson and Chaisson (1997) in the equatorial Atlantic Leg 154. However, Spezzaferri (1994) considered this event diachronous at a regional scale.

In this study, the Top of *G. angulisuturalis* is only recorded in Hole 516F and in Well A, as this species is absent in the other wells. In the lower part of Hole 516F, *G. angulisuturalis* is characterized by a quite regular distribution punctuated by the occurrence of abundance peaks (up to 5%); from 254.77 mbsf, only rare and scattered occurrences are observed and its Top is placed at 236.45 mbsf (Figure 2). In Well A, *G. angulisuturalis* is more discontinuous and slightly less abundant than in Hole 516F; however, it is possible to define a Top level at 2,659.99 m (Figure 3).

4.1.6 | Base of *Globoquadrina dehiscens*

The Base of *G. dehiscens* has been reported as a diachronous event by Spezzaferri (1994), generally occurring in the late Oligocene P22 Zone, except in the Northern Atlantic and in the Mediterranean, where the *G. dehiscens* Base was identified in the early Miocene (lower part of Zone N4). However, Wade et al. (2011) retained this event to define the base of Subzone M1b and calibrated it at 22.44 Ma, on the basis of its position within Chron C6Br at DSDP Sites 516, 522, 563, and 558 and in the Contessa Highway section (Italy; Berggren et al., 1995; Miller et al., 1985; Shackleton et al., 2000).

Typical specimens of *G. dehiscens* are quite common in the upper part of Hole 516F (Figure 8, e–g), where its Base is recorded at 204.32 mbsf (Figure 2). In the Campos Basin wells, *G. dehiscens* is very rare and discontinuously present; however, we recognized its Base in Wells A, B, and C, at 2,640.29; 2,950.35; and 2,717.78 m, respectively (Figures 3–5), whereas in Well D, *G. dehiscens* is present from the base of the studied interval.

4.1.7 | Acme interval of *Tenuitellinata praestainforthi*

Tenuitellinata praestainforthi has five globular chambers in the last whorl and a smooth, nonspinose, and microperforate wall texture. The umbilical area is always covered by a bulla, extending along the sutures. This species is reported from the Oligocene to the early-middle Miocene by Spezzaferri (1994).

Tenuitellinata praestainforthi is very rare in Hole 516F and in Well A, where no particular distribution pattern was identified. Conversely, although poorly represented in all the wells of the Campos Basin, *T. praestainforthi* often exceeds 4% of relative abundance from 2,707.86 m up to the top of Well C, and in Well D, from the base up to 2,703.23 m (Figures 5 and 6), showing an acme interval.

4.1.8 | Top of common *Globigerinoides primordius*

Recently, Spezzaferri et al. (2015) proposed to include *G. primordius* into the new genus *Trilobatus*; however, for the reasons outlined in Appendix A, we prefer to retain this species within the genus *Globigerinoides*. The Base of *G. primordius* was thought to be a reliable marker for the O/Mb (see discussion in Berggren et al., 1985); however, this event was either associated with Chron C8r or Chron C7n in the late Oligocene (Berggren et al., 1995). As for the Base of common *G. primordius*, it is reported to occur within Zone O7 (Wade et al., 2011) and calibrated at 23.50 Ma on the basis of the data of Berggren et al. (1983) and Pujol (1983) from Hole 516F, who observed an abundance increase just below the Base of *P. kugleri* at 215 mbsf.

Similar to the *Globigerinoides* gr., *G. primordius* (Figure 8, h and i) is more abundant in the Campos Basin wells (up to 5.66% in Well A) than in Hole 516F (<1%). The steady distribution pattern of this taxon in Hole 516F (Figure 2) and Well A (Figure 3) below the Base of and the Base of common *P. kugleri* does not allow the recognition of the Base of common *G. primordius*. On the other hand, *G. primordius* shows a decrease in abundance (Tc) in Well C at 2,691.81 m and in Well D at 2,705.48 m (Figures 5 and 6), only showing scattered and rare occurrences above these levels.

4.2 | Calcareous nannofossils

In the examined sites, calcareous nannofossils are common to abundant and preservation is variable from site to site, ranging from medium to very good. The upper Oligocene–lower Miocene calcareous nannofossil assemblage recognized in the five sites is composed of 65 taxa (species and informally subspecies or varieties); the results of the quantitative analyses are reported as percentage values in the range charts (see Data S1), and the most important markers are documented in Figures 9 and 10. We identified a succession of 18 bioevents in the investigated time interval (Table 1) delineated as Base (B), Top (T), Acme Beginning (AB), and Acme End (AE). The reported depths represent the mean depth between the two adjacent samples of each bioevent. A brief discussion of the main bioevents, from the oldest to the youngest, is presented below.

4.2.1 | Top of *Sphenolithus ciproensis*

Sphenolithus ciproensis (Figure 9, e–f) is an easily identifiable small sphenolith, with basal rounded “feet” and a short apical bifurcated spine that is only occasionally preserved. In the literature, the Top of *S. ciproensis* is reported within Chron C7n, with small age differences: 24.43 and 24.35 Ma (base C7n.2n) at the equatorial Pacific Site 1218 (Blaj, Backman, & Raffi, 2009; Blair, 2011), 24.13 Ma (top C7n.2n) at the North Atlantic Site 522 (Shackleton et al., 2000, rescaling Cande & Kent, 1995), and 24.24 Ma (middle part of C7n.2n) at the equatorial Atlantic Sites 925 and 926 (Raffi et al., 2006).

In the lower part of the studied samples of Well A (Figures 2 and 3), the Top of *S. ciproensis* is placed at 2,661.06 m. In Hole 516F, the stratigraphic position of *S. ciproensis* Top cannot be precisely defined because of the presence of an interval of no core recovery (beginning at 254.84 mbsf) just above the last occurrence detected at 254.91 mbsf. We therefore approximate the stratigraphic position of the *S. ciproensis* Top at the mean depth of 253.03 mbsf, between the uppermost sample yielding *S. ciproensis* and the top of the interval of no core recovery (251.16 mbsf; see Table 1).

4.2.2 | Base of *Helicosphaera carteri*

Helicosphaerids are common only at Site 516, whereas they are rarely present in the Campos Basin wells. The Base of *H. carteri* (Figure 10, j), previously indicated in the Iberia Abyssal Plane (de Kaenel & Villa, 1996) as occurring in the upper Oligocene Zone NP25, is recorded at Site 516 at 250.92 mbsf (Figure 2).

4.2.3 | Acme of *Sphenolithus conicus*

The *S. conicus* Acme was identified at Site 1218 in the Pacific Ocean by Blair (2011) from 23.57 to 22.87 Ma and thus encompassing the O/Mb (i.e., with the AE younger than the Top of *S. delphix*).

Sphenolithus conicus (Figure 10, u–v) is present from the base of the studied succession of Well A (Figure 3) showing an upward increasing trend, which delineates an acme interval starting at 2,656.96 m (AB), culminating in a maximum of 24.9% at 2,648.38 mbsf and ending at 2,645.07 m (AE). In Well C, this taxon is less abundant; however, a similar distribution pattern is characterized by the AB at 2,753.275 m, a relative abundance increase up to 14% at 2,747.72 m, and the AE at 2,743.04 m. *S. conicus* is absent in Hole 516F.

4.2.4 | Base and Top of *Sphenolithus delphix*

We have split *S. delphix* (Bukry, 1969) into three varieties differentiated by the total size and the length of the apical spine: *S. delphix* s.l. (short apical spine; Figure 9, m–n); small *S. delphix* (<8 μm; Figure 9, i and j); and *S. delphix* (>8 μm; Figure 9, k and l). Only the last one has a reliable biostratigraphic value. Literature data regarding the distribution range of *S. delphix* show discrepancies: In the Lemme-Carrosio GSSP, the corresponding stratigraphic interval shown in Steininger et al. (1997) was reported from 47 m (within Chron C6Cr) to 31 m (within Subchron C6n.1r), although Aubry and Villa (1996) in the same section reported only rare and discontinuous presence from just below the boundary up to Subchron C6n.1r. However, the preservation and the rare occurrence of sphenoliths in the Neogene base stratotype section shed doubts on the real distribution of *S. delphix*. The recent age calibrations by Gradstein et al. (2012, North Atlantic) and Backman et al. (2012, equatorial Pacific) are 23.21 and 23.38 Ma for the Base and 23.11 and 23.06 Ma for the Top, respectively. Gradstein et al. (2012) used data from Raffi et al. (2006) and Shackleton et al. (2000, North Atlantic), who however report ages more comparable to that of Backman et al. (2012). The corresponding position in the GPTS varies from the upper part of C6Cr to the lower part of C6Cn.2r for the Base and within C6Cn.2r for the Top. Backman et al. (2012) use the Top of *S. delphix* to define the base of CNM1, which precedes the O/Mb (23.03). Although the *S. delphix* Top is generally indicated in Subchron C6Cn.2r (Backman et al., 2012), in DSDP Site 563, it occurs in the basal portion of C6Cn.2n (Maiorano & Monechi, 1998; Miller et al., 1985).

Sphenoliths are less abundant in Hole 516F; however, we recognized the Base of *S. delphix* at 229.8 mbsf, whereas the Top falls in an interval of no core recovery that range between 226.35 and 218.59 mbsf (midpoint at 222.47 mbsf, Figure 2). Sphenoliths are more abundant in the Campos Basin: In Well A, the Base and the Top were identified at 2,651.635 and 2,648.165 m, respectively (Figure 3); in Well C, the short distribution range of *S. delphix* occurs from 2,749.575 m (B) to 2,744.85 m (T; Figure 5). We remark that smaller morphotypes are present in older sediments.

4.2.5 | Base and Top of *Sphenolithus disbelemnus* <4 μm

Sphenolithus disbelemnus was defined by Fornaciari (1996) as a small sphenolith ranging in size from 3 to 4 μm. It had priority on

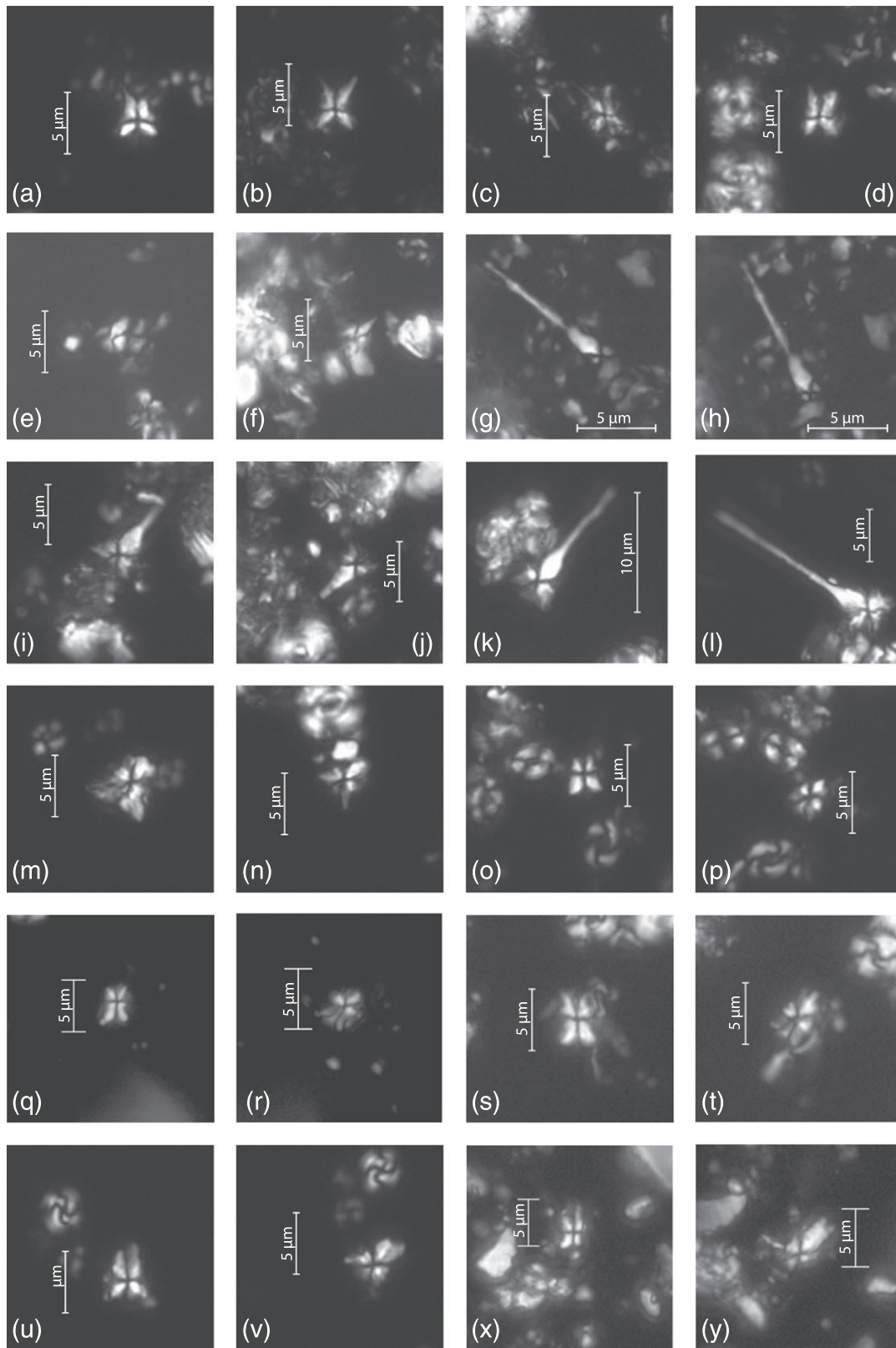


FIGURE 9 (a and b) *Sphenolithus capricornutus*, X Nicols, 100X (sample 516F-5-7 0–2 cm, 215.8 mbsf); (c and d) *S. capricornutus* XN, 100X (sample 516F-5-7 36–38 cm, 216.16 mbsf); (e and f) *S. cipoensis*, XN, 100X (Sample 516F-11-2 53–55 cm, 266.13 mbsf); (g and h) *Sphenolithus cf. S. pseudoheteromorphus* XN, 100X (Well C 2,707.2 m); (i and j) *S. delphix*, XN, 100X (sample 516F-7-1 139–141 cm, 227.49 mbsf); (k and l) *S. delphix*, XN, 100X (Sample 516F-7-1 60–62 cm, 226.7 mbsf); (m and n) *S. delphix* (short apical spine), XN, 100X (Sample 516F-8-4 9–11 cm, 240.19 mbsf); (o and p) *S. disbelemnus* (<4 μm), XN, 100X (Sample 516F-6-1 4–6 cm, 216.64 mbsf); (q and r) *S. disbelemnus* > 4 μm , XN, (Well A, Sample 2,636.75 m); (s) *S. cometa*, XN, 100X (Well D, Sample 2,697.22 m); (t) *S. cometa*, XN, 100X (Sample 516F 3–3 56–58 cm); (u and v) *S. procerus*, XN, 100X (Sample 516F-6-2 49–51 cm, 218.59 mbsf); (x and y) *S. cometa*, XN (Well A, Sample 2,636.75 m)

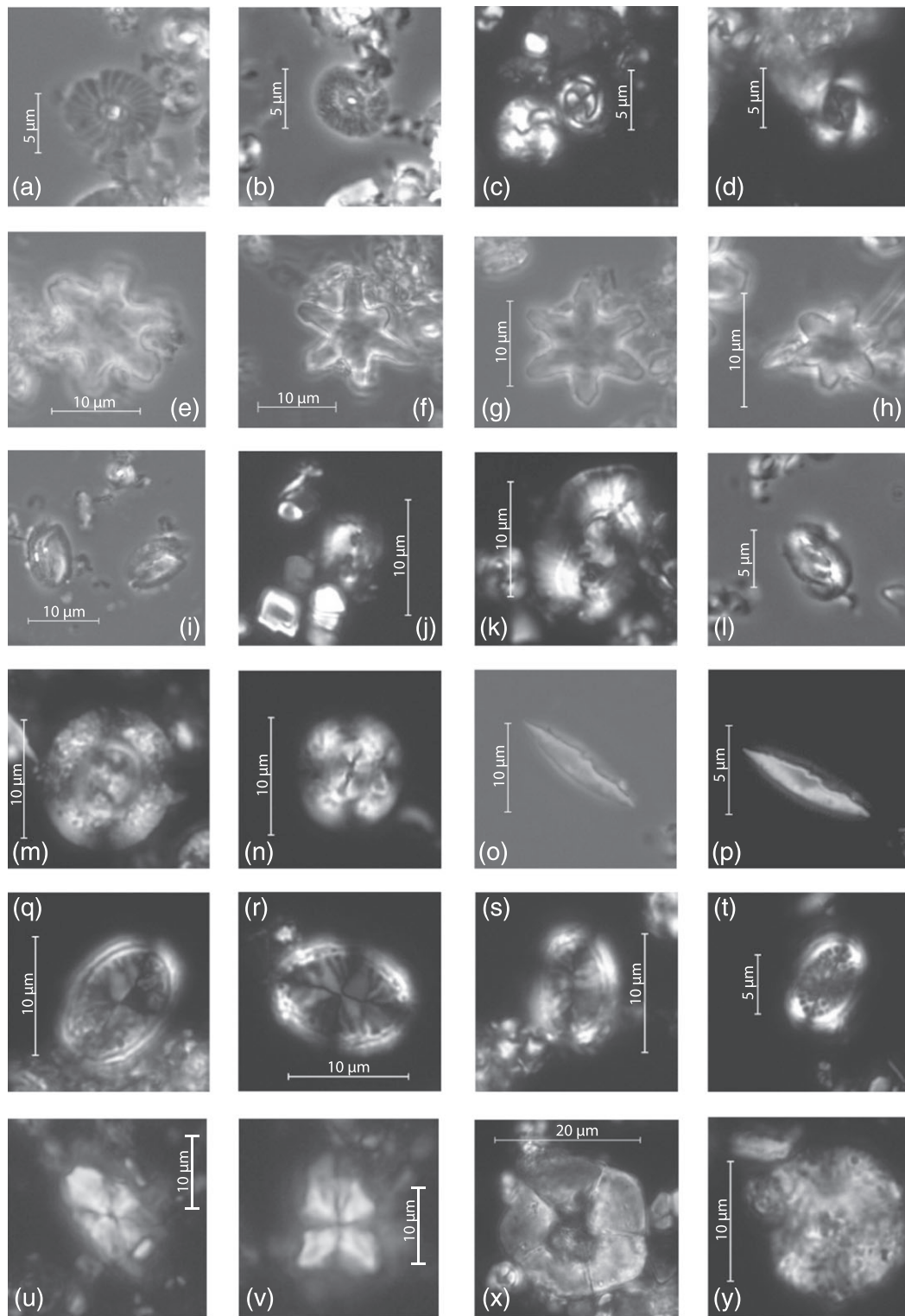


FIGURE 10 (a and b) *Calcidiscus pataecus*, phase contrast, 100X, (Sample 516F-5-6 118–120 cm, 215.78 mbsf); (c) *C. subdisticus*, X Nicols, 100X (Sample 516F-9-1 104–106 cm, 246.14 mbsf); (d) *Reticulofenestra lockeri*, XN, 100X (Sample 516F-6-1 18–20 cm, 216.78 mbsf); (e–g) *Discoaster druggii*, PC, 100X (Sample 516F-3-1 8–10 cm, 188.18 mbsf); (h) *D. druggii* small, PC, 100X (Sample 516F-3-1 110–112 cm, 189.20 mbsf); (i) *Helicosphaera obliqua*, PC, 100X (Sample 516F-8-7 66–68 cm, 245.00 mbsf); (j) *H. carteri*, X N, 100X (Sample 516F-9-4 120–122 cm, 250.80 mbsf); (k) *H. rhomba*, XN, 100X (Sample 516F-5-4 142–144 cm, 213.02 mbsf); (l) *H. vedderi*, PC, 100X (Sample 516F-5-5 78–80 cm, 213.88 mbsf); (m and n) *Dictyococcites bisectus*, XN, 100X (Sample 516F-9-4 21.5–23.5 cm, 249.815 mbsf); (o and p) *Triquetrorhabdulus carinatus*, PC and XN, 100X (Sample 516F-3-1 8–10 cm, 188.18 mbsf); (q–s) *Pontosphaera wallacei*, XN, 100X (Sample 516F-8-7 66–68 cm, 245.00 mbsf); (t) *P. callosa*, XN, 100X (Sample 516F-5-6 8–10 cm, 214.68 mbsf); (u and v) *Sphenolithus conicus*, XN, 100X (Well A, Sample 2,640.84 m); (x) *Braarudosphaera bigelowii*, XN, 100X (Sample 516F-9-3 98.5–100.5 cm, 249.085 mbsf); (y) *Cyclicargolithus abisectus*, XN, 100X (Sample 516F-11-1 141–143 cm, 265.51 mbsf)

TABLE 1 Summary of the key bioevents used in the studied successions with depths and magnetostratigraphic position according to the new magnetostratigraphy of Hole 516F (see also Florindo et al., 2015)

Code	Event	Campos Basin												Rio Grande Rise 516F			
		Well A			Well B			Well C			Well D			Bottom	Mean depth	Chron (this study)	
		Top	Bottom	Mean depth	Top	Bottom	Mean depth	Top	Bottom	Mean depth	Top	Bottom	Mean depth				
T	B S. disbelemnos (<4 µm)	-	-	-	-	-	-	-	-	-	-	-	-	-	-	-	-
12	AE T. praestainforthi	-	-	-	-	-	-	-	-	-	-	-	-	-	-	-	-
11	Tc G. primordius	2,691.65	2,691.97	2,691.81	2,705.13	2,705.83	2,705.48	2,705.83	2,706.13	2,705.98	2,705.83	2,706.13	2,705.98	191.34	191.71	191.525	CBn.2n base
S	T S. disbelemnos	-	-	-	-	-	-	-	-	-	-	-	-	-	-	-	-
R	B S. cometa	2,699.95	2,701.08	2,700.515	2,706.98	2,707.23	2,707.1	2,706.98	2,707.23	2,707.1	2,706.98	2,707.23	2,707.1	-	-	-	-
Q	B S. procerus	2,701.08	2,701.6	2,701.34	2,707.23	2,707.53	2,707.38	2,707.23	2,707.53	2,707.38	2,707.23	2,707.53	2,707.38	-	-	-	-
P	T Sphenolithus. cf. S. pseudoheteromorphus	2,702.77	2,703.37	2,703.07	2,710.88	2,711.13	2,711.005	2,710.88	2,711.13	2,711.005	2,710.88	2,711.13	2,711.005	-	-	-	-
O	B Sphenolithus. cf. S. pseudoheteromorphus	2,707.2	2,707.67	2,707.435	-	-	-	-	-	-	-	-	-	-	-	-	-
10	AB T. praestainforthi	2,707.67	2,708.05	2,707.86	2,721.20	2,721.20	2,721.20	2,707.67	2,708.05	2,707.86	2,721.20	2,721.20	2,721.20	194.00	194.31	194.155	C6Bn.2n base
N	B S. disbelemnos	2,636.75	2,637.025	2,637.025	2,947.77	2,948.52	2,948.15	2,947.77	2,948.52	2,948.15	2,947.77	2,948.52	2,948.15	196.38	196.68	196.53	C6Br top
M	B D. druggii	-	-	-	-	-	-	-	-	-	-	-	-	204.23	204.41	204.32	C6Cn.1n base
9	B G. dehiscentis	2,640.18	2,640.4	2,640.29	2,950.27	2,950.42	2,950.345	2,950.27	2,950.42	2,950.345	2,950.27	2,950.42	2,950.345	204.23	204.41	204.32	CC6Cn.1n base
8	Paracme end G. ciproensis gr.	-	-	-	-	-	-	-	-	-	-	-	-	-	-	-	-
L	AB T. carinatus	-	-	-	-	-	-	-	-	-	-	-	-	204.23	204.41	204.32	C6Cn.1n base
I	B D. druggii (10–15 µm)	2,642.18	2,642.41	2,642.295	-	-	-	-	-	-	-	-	-	-	-	-	-
H	AE S. conicus	2,644.93	2,645.21	2,645.07	-	-	-	-	-	-	-	-	-	-	-	-	-
G	T S. capricornutus	2,646.05	2,646.33	2,646.19	-	-	-	-	-	-	-	-	-	-	-	-	-
7	Bc P. kugleri	2,646.33	2,646.65	2,646.49	2,740	2,740.75	2,740.38	2,740	2,740.75	2,740.38	2,740	2,740.75	2,740.38	213.88	214.68	214.28	C6Cn.2n base
F	T S. delphix	2,647.95	2,648.38	2,648.165	2,744.65	2,745.05	2,744.85	2,744.65	2,745.05	2,744.85	2,744.65	2,745.05	2,744.85	218.59	226.35	222.47	-
6	Br Globigerinoides gr.	2,649.68	2,650.23	2,649.96	2,747.3	2,747.72	2,747.51	2,747.3	2,747.72	2,747.51	2,747.3	2,747.72	2,747.51	229.11	229.285	229–197	-
E	B S. disbelemnos (<4 µm)	2,650.93	2,651.3	2,651.115	2,748.8	2,749.4	2,749.1	2,748.8	2,749.4	2,749.1	2,748.8	2,749.4	2,749.1	-	-	-	-
D	B S. delphix	2,651.49	2,651.78	2,651.635	2,749.4	2,749.75	2,749.575	2,749.4	2,749.75	2,749.575	2,749.4	2,749.75	2,749.575	229.65	229.95	229.8	C6Cr top?
C	AB S. conicus	2,656.79	2,657.13	2,656.96	2,753.05	2,753.50	2,753.275	2,753.05	2,753.50	2,753.275	2,753.05	2,753.50	2,753.275	-	-	-	C6Cr*
5	T G. angulituralis	2,659.82	2,657.13	2,659.99	-	-	-	-	-	-	-	-	-	236.18	236.72	236.45	C6Cr
B	B H. carteri	-	-	-	-	-	-	-	-	-	-	-	-	250.8	251.035	250.92	C7n.1n
A	T S. ciproensis	2,660.52	2,661.61	2,661.06	-	-	-	-	-	-	-	-	-	251.16	254.91	253.03	C7n
4	G. ciproensis gr. abundance drop	-	-	-	-	-	-	-	-	-	-	-	-	paracme base	-	-	-
		2,661.61	2,662.2	2,661.91	251.16	254.77	252.97	251.16	254.77	252.97	251.16	254.77	252.97	251.16	254.77	252.97	C7n
3	B Globigerinoides gr.	2,663.25	2,664.23	2,663.74	256.3	256.55	256.43	256.3	256.55	256.43	256.3	256.55	256.43	265.19	265.51	265.35	C7n.2n base
2	T G. testarugosa	-	-	-	266.13	266.38	266.26	266.13	266.38	266.26	266.13	266.38	266.26	266.13	266.38	266.26	C7r
1	B P. kugleri	-	-	-	-	-	-	-	-	-	-	-	-	-	-	-	-

Note. Asterisks refer to bioevents only present in the Campos Basin, for which the magnetostratigraphic position is derived by the projection of the events on Hole 516F. Following Backman et al. (2012) and Raffi et al. (2006), bioevents are indicated as B = Base; Bc = Base common occurrence; Br = Base regular occurrence; T = Top; Tc = Top common occurrence; PE = Paracme beginning; PB = Paracme end; AB = Acme beginning; and AE = Acme end.

Sphenolithus aubryae described later the same year by de Kaenel and Villa (1996) who, however, indicated a range in size between 3.5 and 4.5 μm . In our samples, we recognized two dominant sizes of this species; thus, we keep separated forms $<4 \mu\text{m}$ from those $>4 \mu\text{m}$.

The small morphotype first appears above the *S. delphix* Base, whereas the bigger morphotype is present above the O/M boundary and its stratigraphic range is comparable to that of *S. disbelemnos* as reported by Backman et al. (2012).

The Base of the small morphotype is observed in Wells A and C at 2,651.115 and 2,749.1 m, respectively (Figures 3 and 5). However, at the beginning of its range, it occurs in low abundance and its detection requires careful analyses. In Well D, it is still present above the Top of *S. disbelemnos* $>4 \mu\text{m}$, and it last occurs at 2,694.59 m (Figure 6). In Hole 516F, the scarce presence of sphenoliths hinders the identification of this event.

4.2.6 | Top of *Sphenolithus capricornutus*

Though occurring with rare and discontinuous specimens, the Top of *S. capricornutus* (Figure 9, a–d) may be useful to approximate the O/Mb, because in the Lemme-Carrosio section (Aubry & Villa, 1996), it was positioned within the range of *S. delphix*, and in Site 563, it was recognized together with the Top of *S. delphix* (Maiorano & Monechi, 1998). Gradstein et al. (2012) report, for this event, an age of 22.97 Ma (ODP Leg 145), within Subchron C6Cn.2n.

This sphenolith is quite rare in the studied successions ($<1\%$) and only in Well A that *S. capricornutus* shows a continuous distribution up to its Top, which occurs at 2,646.19 mbsf (Figure 3). In Well C and in Hole 516F, *S. capricornutus* is very rare, but the Base was tentatively placed at 2,748.095 m in Well C (Figure 5), and at 215.79 mbsf in Hole 516F (Figure 2).

4.2.7 | Base of *Discoaster druggii* (10–15 μm)

In de Kaenel and Villa (1996), *D. druggii* was differentiated into small (10–15 μm ; Figure 10, h) and large ($>15 \mu\text{m}$; Figure 10, e–g) morphotypes: The latter corresponds to the original description of Bramlette and Wilcoxon (1967) and marks the base of Zone NN2. The small variety was said to occur just above the O/Mb, as observed by de Kaenel and Villa (2010) in the Lemme-Carrosio section.

In Well A, small *D. druggii* is present with abundance between 0.2% and 0.4%, and its Base occurs at 2,642.295 m (Figure 3). In Well C, the small *D. druggii* is present with abundances ranging between 0.2% and 1.2%, from 2,728.68 m up to the top; however, its Base is not traceable with certainty, as the sample that contains the first small *D. druggii* is just above an interval of no core recovery (Figure 5). *D. druggii* (10–15 μm) is not recognized in Hole 516F.

4.2.8 | Acme interval of *Triquetrorhabdulus carinatus*

In Backman et al. (2012), the distribution pattern of *T. carinatus* shows several abundance fluctuations (acme intervals) in its upper range (see fig. 4 in Backman et al., 2012) and a sudden drop at the topmost part of Subchron C6Bn.2n, prior to its extinction.

Triquetrorhabdulus carinatus (Figure 10, o–p) is present throughout the study succession in Hole 516F (Figure 2); in particular, it increases in abundance from 204.32 mbsf (AB) and is common up to the top of

studied section. This species is very rare in the Campos Basin wells, and no relevant abundance fluctuations were detected.

4.2.9 | Base of *Discoaster druggii*

Discoaster druggii (Figure 10, e–g) is described as a large discoaster whose total length is $>15 \mu\text{m}$ (Bramlette & Wilcoxon, 1967). The Base of *D. druggii* defines the base of NN2 of Martini (1971) and the base of CN1b of Okada and Bukry (1980), but its biostratigraphic value has been questioned, as in several environments, it is too sporadic or absent (e.g., Rio, Fornaciari, & Raffi, 1990). Recently, Backman et al. (2012) discarded this bioevent as a zonal marker, being diachronous at a global scale. However, these authors indicate that the Base of *D. druggii* occurs in Zone CNM1 and assign it an age of 22.59 Ma in Chron C6Br, between the Top of *S. delphix* and the Base of *S. disbelemnos*, (see also Pälke et al., 2005; Site 1218). The same magnetostratigraphic position was observed at Sites 563 (Maiorano & Monechi, 1998). Instead, in the Eastern Mediterranean, this event is astronomically dated at 22.80 Ma and falls in Subchron C6Cn.1r (Lourens et al., 2004).

In our material, *D. druggii* has been recognized only at Site 516, where its Base is recorded at 196.53 mbsf (Figure 2).

4.2.10 | Base and Top of *Sphenolithus disbelemnos* $>4 \mu\text{m}$

In Hole 516F, rare specimens of *S. disbelemnos* $>4 \mu\text{m}$ (Figure 9, q and r) have been detected from 194.155 m (Base), just above the Base of *D. druggii* (Figure 2) and correlated with Subchron C6Bn.2n. In Well A, the Base of *S. disbelemnos* $>4 \mu\text{m}$ is recognized above the Base of *D. druggii* 10–15 μm , at 2,637.025 m, with rare and discontinuous distribution (Figure 3), whereas in Well B, the Base occurs at 2,948.15 m (Figure 4). In Well C, the Base is located at 2,721.21 m, just above an interval of no core recovery and a few meters of sandstones barren in microfossils (Figure 5), so that a lower occurrence cannot be ruled out. *S. disbelemnos* $>4 \mu\text{m}$ is present up to the top in Wells A, B, and C, whereas the Top is only identified in Well D at 2,705.98 m.

According to Backman et al. (2012), Figure 3, at Site 1218, the Base of *S. disbelemnos* occurs just above the Base of *D. druggii*, in Chron C6Br with an age of 22.48 Ma (age recalibrated to the GPTS of Gradstein et al., 2012) and it defines the base of Zone CMN2. Conversely, Fornaciari and Rio (1996) and Aubry and Villa (1996), not finding *D. druggii* in the Mediterranean realm, assume the position of the *S. disbelemnos* Base in Zone NN1, as well as Maiorano and Monechi (1998) at Site 563 and Shackleton et al. (2000) at Site 522, who place it in the uppermost Zone NN1, close to the C6Cn.1r/C6Cn.1n boundary. We think that our *S. disbelemnos* $>4 \mu\text{m}$ is comparable with the range of *S. disbelemnos* of Backman et al. (2012), even though the latter was defined up to 4 μm , whereas the small morphotype is rare and difficult to detect.

4.2.11 | Base and Top of *Sphenolithus cf.*

S. pseudoheteromorphus

Sphenolithus pseudoheteromorphus was first described by Fornaciari and Agnini (2009) at the top of the Burdigalian Zone NN2 in Chron C6n. Here, we detected a small sphenolith, with a bright apical spine at 45° that differs from *S. pseudoheteromorphus* and from *S. delphix* in

having a longer apical spine and the absence of long basal spines. Therefore, the specimens with these features have been kept separate from *S. pseudoheteromorphus*, which is reported by Fornaciari and Agnini (2009) as occurring in a younger interval, and informally named *Sphenolithus* cf. *S. pseudoheteromorphus* (Seirin Shimabukuro pers.com., 2013; Figure 9, g and h). The Base of *Sphenolithus* cf. *S. pseudoheteromorphus* is recognized only in Well C at 2,707.435 m (Figure 5). The Top of *Sphenolithus* cf. *S. pseudoheteromorphus* (Figure 9, g and h) is recognized in Wells C and D at 2,703.07 m and 2,711.005 m, respectively (Figures 5 and 6). The few specimens recovered in the uppermost part of Well D, above the Top, are considered as reworked.

4.2.12 | Base of *Sphenolithus procerus*

When the apical spine is oriented at 0°, *S. procerus* shows a shape that reminds a bottle and could be confused with *S. cometa*, from which it is distinguished by the absence of the flaring apical spines. *Sphenolithus procerus* has short basal elements and extended apical spines that at 0° appear as two elements separated by a central suture, while at 45°, it is distinguished from *S. cometa* by its thinner apical spine. Intermediate forms between *S. cometa* and *S. procerus* are often present, and the elongated apical spines of *S. cometa* are diagnostic to separate the two species. Maiorano and Monechi (1998) place this event above the Base of *S. cometa* in Chron C6Aa at DSDP Site 563.

Sphenolithus procerus is only present in Wells C and D with rare but well-preserved specimens (Figures 5 and 6), and its Base is documented shortly below the Base of *S. cometa*, at 2,701.34 and 2,707.38 m, respectively (Figure 9, u and v).

4.2.13 | Base of *Sphenolithus cometa*

Sphenolithus cometa (Figure 9, s, t, x, and y) is a small-medium sphenolith with a short narrow base and a long diverging apical spine, whose elements are longitudinally separated to form three to four elongated spines that flare upwards. At 45°, the tripartite apical spine shows a decreasing birefringence from the base. *Sphenolithus cometa* looks similar to *S. disbelemnus* when the apical spine is at 0°, but in the latter, the four basal elements (two long and two short) are almost parallel. *Sphenolithus dissimilis* also possesses a spine formed by three elements, but they are shorter and not separated longitudinally like the apical elements of *S. cometa*. In our samples, the specimens of this taxon are rare and the identification may be difficult in poorly preserved material. The Base of *S. cometa* was previously documented only by de Kaenel and Villa (1996) in NN2 and by Maiorano and Monechi (1998) at the top of Subchron C6Bn.2n at Site 563; we detected this event in the same subchron in Hole 516F at 191.525 mbsf (Figure 2). In Wells C and D, this event has been recorded just above the Base of *S. procerus* (Figure 5) at 2,700.515 and 2,707.1 m, respectively (Figure 6).

4.3 | Magnetostratigraphy

Although NRM intensities are generally low throughout the core, step-wise AF demagnetization enabled isolation of the ChRM component for most of samples analyzed, which allowed construction of a magnetic polarity zonation. The ChRM inclinations enable delineation of

eight magnetozones that are defined using at least two consecutive samples with inclinations distinctly different from neighboring intervals. In some magnetozones, occasional isolated samples have polarities opposite to those of the rest of the magnetozone. Such isolated samples are not used to define polarity zones. Magnetozones are labeled according to their polarity (N = normal or R = reversed), with progressive down-core numbering within the hole. We used the GPTS of Gradstein et al. (2012) to develop an age model for the studied interval. Our magnetostratigraphic interpretation for Hole 516F is based on the biostratigraphic data detailed above and is presented in Figure 11 (see also Florindo et al., 2015).

5 | HIGH-RESOLUTION INTEGRATED CALCAREOUS PLANKTON BIOSTRATIGRAPHY AND MAGNETOSTRATIGRAPHY OF THE SOUTHWESTERN ATLANTIC

The planktonic foraminiferal and calcareous nannofossil events (Table 1), identified through high-resolution quantitative analyses, allowed us to correlate in detail the Campos Basin wells with the bio-magnetostratigraphic record of DSDP Hole 516F and to obtain an integrated high resolution biostratigraphic framework for the entire investigated stratigraphic interval (Figure 12). Furthermore, we stress the presence and importance of several regional bioevents that were only observed in the Campos Basin or in Hole 516F and were previously unreported or overlooked in literature.

The presence of *P. pseudokugleri* from the base of the investigated successions, the appearance of *P. kugleri* and *G. dehiscens*, and the presence of *P. kugleri* up to the top indicate that the entire succession can be referred to the interval encompassing the planktonic foraminiferal Zone O7 (*pars*) to Subzone M1b (*pars*) of Wade et al. (2011). The presence of *S. ciperoensis* from the base and of *S. disbelemnus* > 4 µm and *S. cometa* at the top of the investigated successions indicate an interval including the nannofossil Zones NP25 (*pars*) to NN2 (*pars*; Martini, 1971) or CNO5 (*pars*; Agnini et al., 2014) to CNM3 (*pars*) of Backman et al. (2012).

The oldest investigated sediments are younger than the Base of *P. pseudokugleri* (25.21 Ma, Gradstein et al., 2012) and the Top of common *C. abisectus* (24.67 Ma, Lyle et al., 2002), as the former is present and the latter is rare in the basal portions of Hole 516F and Well A. The presence of *P. pseudokugleri* up to the top of the studied interval (Well D) indicates an age older than 21.31 Ma (Gradstein et al., 2012) for the top of the succession.

The correlation of the Campos Basin wells with Hole 516F was possible thanks to the identification of several bioevents present in both areas. However, calcareous plankton assemblages also show differences in taxonomic compositions and/or relative abundances of some taxa, which indicates a certain degree of provincialism, probably due to different palaeoceanographic conditions; as a consequence, some bioevents cannot be used to correlate the two areas.

The stratigraphic position of the Base of the *Globigerinoides* gr. (below) and the Top of *S. ciperoensis* (above), both occurring in Chron C7n, allows to correlate the lower portions of Well A and Hole 516F (Figure 12). Although the recognition of the Base of *S. ciperoensis* is

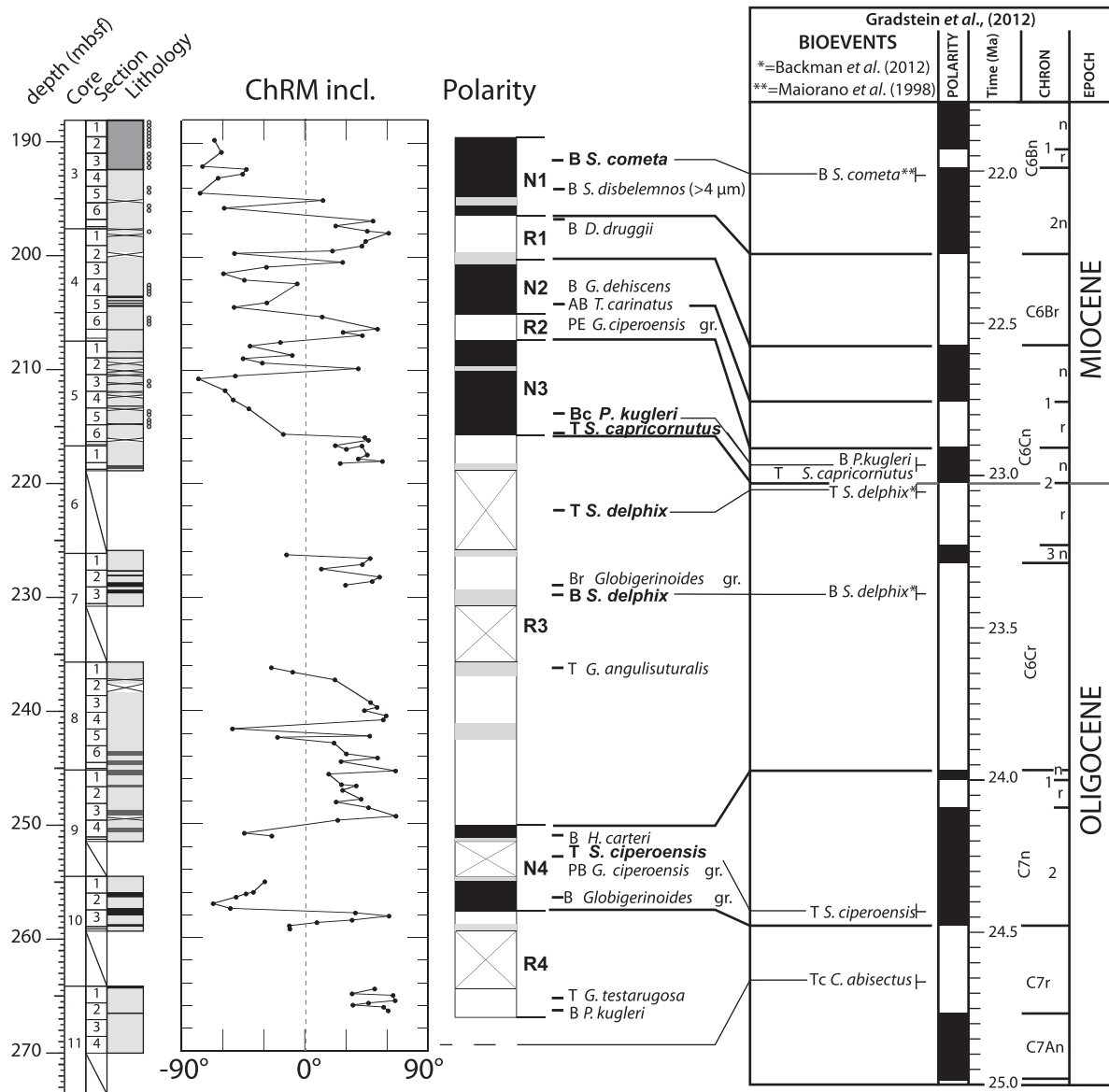


FIGURE 11 Correlation of the new magnetic polarity zonation of Hole 516F with the GPTS of Gradstein et al. (2012) through the selected bioevents (in bold) identified in Hole 516F. Black (white) indicates normal (reversed) polarity

complicated by the interval of no core recovery between 259.5 and 264 mbsf, the magnetostratigraphic position of this event is in good agreement with that reported in the literature (Blair, 2011; Blaj, Backman, & Raffi, 2009; Raffi et al., 2006 and Shackleton et al., 2000) in Chron C7n. Additionally, the PB of the *G. ciproensis* gr. falls in the same no-recovery interval; its position is better constrained in Well A, where the corresponding AD occurs between the Base of the *Globigerinoides* gr. and the Top of *S. ciproensis*. Both the PB and AD of the *G. ciproensis* gr. are previously unreported in literature. Conversely, in the lower part of the studied successions, the *G. angulituralis* Top and the *H. carteri* Base and the *G. testarugosa* Top are only present in Hole 516F, within Subchron C7n.1n and Chron C7r, respectively.

The Base and Top of *S. delphix*, the Base of regular *Globigerinoides* gr., the Top of *S. capricornutus*, and the Base of common *P. kugleri*, all occurring in a relatively short stratigraphic interval, allowed the correlation between the Campos Basin wells (A and C) and Hole 516F

across the O/Mb. Following the formal definition of the boundary in the GSSP (Steininger et al., 1997), in Hole 516F, the O/Mb is placed at the base of Subchron C6Cn.2n, which is approximated by the Top of *S. delphix* (below) and by the Top of *S. capricornutus* and Base of common *P. kugleri* (above). The magnetostratigraphic position of the Base of common *P. kugleri* and its relative position above the *S. delphix* Top and close to the of *S. capricornutus* Top, indicate that the Base of common *P. kugleri* can be considered time-equivalent to the Base of *P. kugleri* recorded in the Lemme-Carrosio section (Steininger et al., 1997) and at low latitude (Leg 154, Pearson & Chaisson, 1997); therefore, in this study, this bioevent is used to define the base of Zone M1 (Wade et al., 2011). We note that the *S. capricornutus* Top occurs either slightly below or above the Base of common *P. kugleri* in Hole 516F and Well A, respectively; conversely, in Well C, this event occurs within the range of *S. delphix*. However, notwithstanding its extreme scarcity, the *S. capricornutus* Top can be useful to approximate the O/Mb. In the absence of

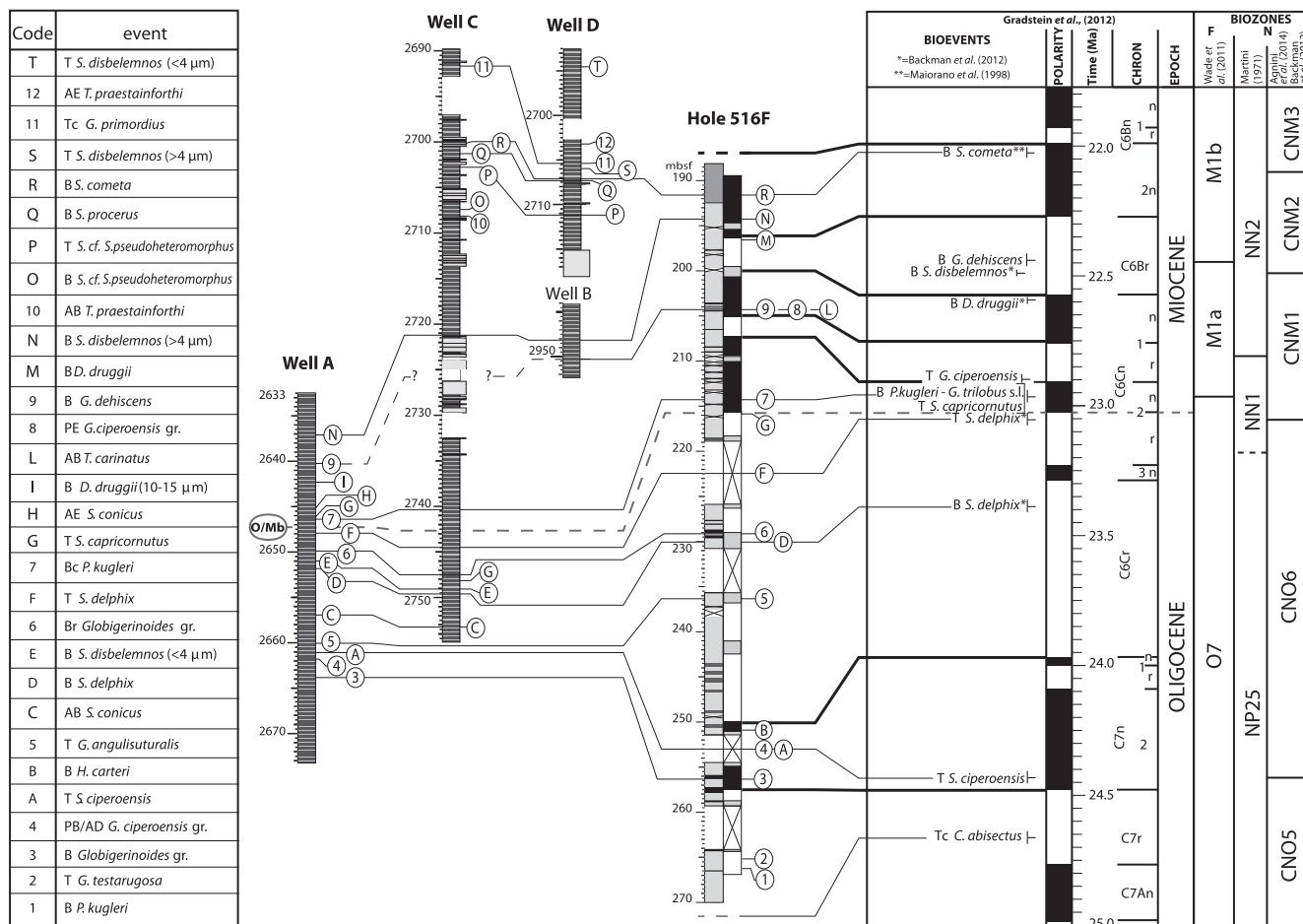


FIGURE 12 Bio-magnetostratigraphic correlation between the Campos Basin wells, Hole 516F and the GPTS of Gradstein et al. (2012); the bioevents in the GPTS are from Maiorano and Monechi (1998), Backman et al. (2012), and Gradstein et al. (2012). The grey dashed line represents the O/Mb. The codes of the bioevents are also reported in Table 1. Bold lines refer to the magnetostratigraphic correlation between Hole 516F and the GPTS

magnetostratigraphy, in the Campos Basin wells, the base of the Miocene is placed at the midpoint between the Top of *S. delphix* and the Base of common of *P. kugleri*. Moreover, the correlation between Wells A and C by means of *S. delphix* Base and Top is strengthened by the occurrence of the AB of *S. conicus* and the Base of *S. disbelemnus* (<4 μm), below and within the *S. delphix* range, respectively (Figure 11).

The correlation of the upper part of the studied interval of Hole 516F and of the Campos Basin wells is based on the identification in both areas of the Bases of *G. dehisces*, *S. disbelemnus* >4 μm, and *S. cometa*. In Hole 516F, the *G. dehisces* Base is associated with Subchron C6Cn.1n and predates the Bases of *S. disbelemnus* >4 μm and of *S. cometa*, both within Subchron C6Bn.2n. In the Campos Basin, the same order of bioevents is observed in Wells A and B, whereas the *G. dehisces* Base postdates the *S. disbelemnus* >4 μm Base in Well C (Figure 5). The delayed Base of *G. dehisces* in Well C could be due to a combination of the rarity and scattered distribution of the species, the presence of sandstone intercalations and of no core recovery intervals below the Base of *S. disbelemnus* >4 μm. Also, in this stratigraphic interval, the occurrence of some bioevents is restricted only to one studied area. In Hole 516F, the PE of *G. ciproensis* gr. (associated with

the base of Subchron C6Cn.1n) and the Base of *D. druggii* (occurring at the top of Chron C6Br) predate the *S. disbelemnus* Base, whereas they are not recorded in Campos Basin wells. On the contrary, *S. cf. pseudoheteromorphus* and *S. procerus* are only present in the Campos basin and allowed the correlation of the upper portion of Wells C and D, where they are included within the acme of *T. praestainforthi* and constrained at the top by the Base of *S. cometa* (in Subchron C6Bn.2n in Hole 516F). *Sphenolithus procerus* is absent in Hole 516F, and thus, its Base is considered a useful bioevent only in the Campos Basin, where it occurs below the *S. cometa* Base, and not above, as documented in the North Atlantic Site 563 (Maiorano & Monechi, 1998).

The uppermost part of Well D is younger than the top of the studied interval of Hole 516F; here, we recorded additional bioevents: the Top of *S. disbelemnus*, the Top of common *G. primordius* (also at the top of Well C), the AE of *T. praestainforthi*, and the Top of *S. disbelemnus* (<4 μm), all previously unreported in the literature. This uppermost portion of Well D is also characterized by a decreasing abundance trend of *P. pseudokugleri* and *P. kugleri*, possibly heralding their Tops, calibrated at 21.31 and 21.12 Ma (Gradstein et al., 2012), respectively.

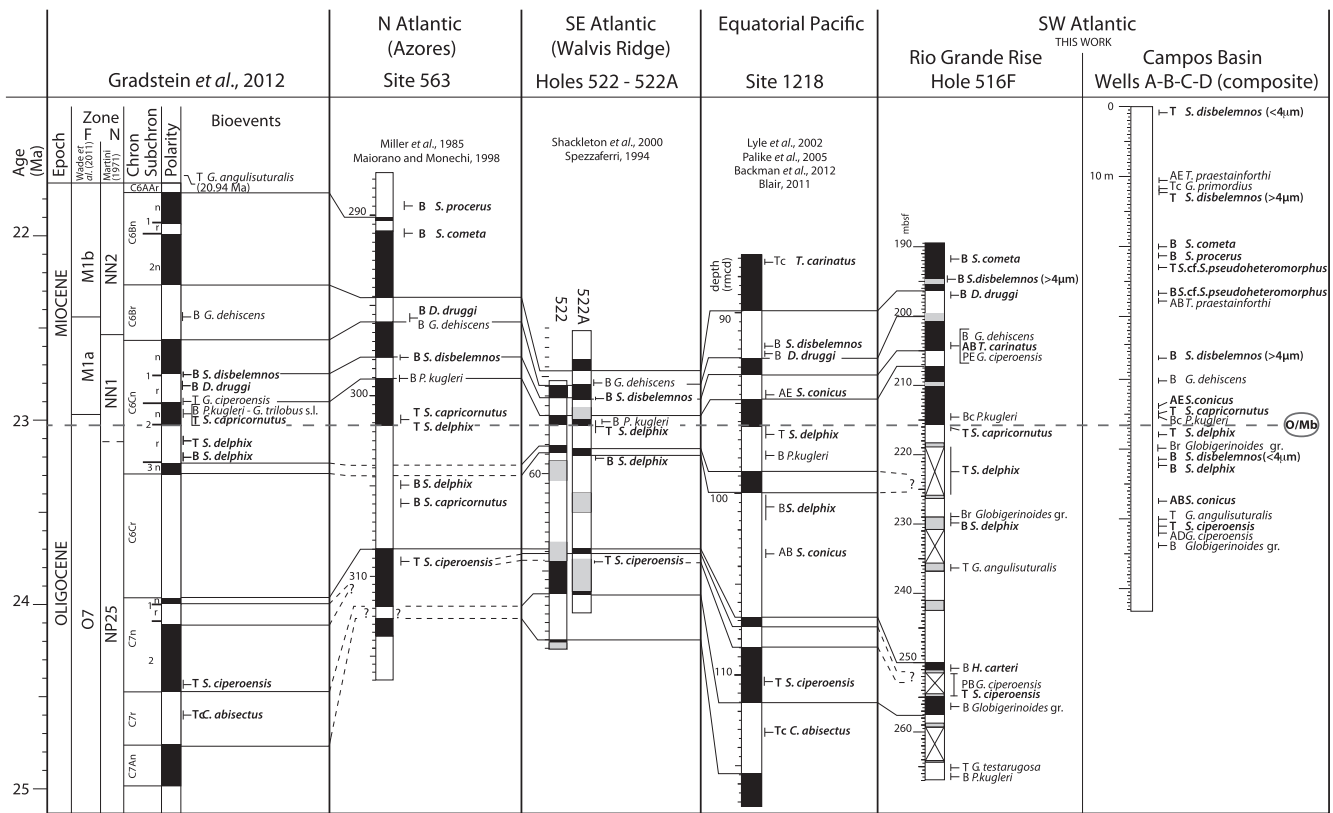


FIGURE 13 Comparison of the OMT between the GPTS and the bioevents compiled in Gradstein et al. (2012), the bio-magnetostratigraphy of ODP Site 1218 and DSDP Sites 563 and 522 and our results. The position of *S. disbelemnos* top is reported as in fig. 3 of Backman et al. (2012), which is different from the depth in tab. 2 of the same work. The grey dashed line represents the O/Mb (i.e., base of Subchron C6Cn.2n)

6 | ADDITIONAL REMARKS ON THE OMT CALCAREOUS PLANKTON BIOSTRATIGRAPHY

The calcareous plankton biostratigraphy of the Campos Basin and the bio-magnetostratigraphy of Hole 516F motivate a discussion of the most relevant bioevents arising from the comparison of our results with previous studies focused on the OMT interval (Figure 13).

Paragloborotalia kugleri Base and Base common occurrence – The distribution pattern of *P. kugleri* resulting from this study, integrated with the magnetostratigraphy and the calcareous nannofossil biostratigraphy of Hole 516F, indicates that the lowest occurrence of rare specimens of this species is associated with Chron C7r and well predates the *S. ciproensis* Top. A late Oligocene age for the Base of *P. kugleri* results when the quantitative data of Spezzaferri (1992, 1994) from Hole 516F are framed in our new bio-magnetostratigraphy and the GSSP criteria to identify the that O/Mb (Steininger et al., 1997) is adopted. Furthermore, a late Oligocene Base of *P. kugleri*, although from younger levels, is reported by Keller (1981) from DSDP Hole 292 approximately 5.6 m above the Top of *S. ciproensis* (Ellis, 1975), and by Lyle et al. (2002) from Site 1218 (equatorial Pacific) associated with the youngest Oligocene Subchron C6Cn.2r. However, these data are in contrast

with the widely accepted literature data according to which the Base of *P. kugleri* is associated with Subchron C6Cn.2n and approximates the O/Mb, as depicted by Steininger et al. (1997). Considering the bio-chronostratigraphic importance of this event at the OMT and the above-mentioned discrepancies, it is clear that further discussions on the criteria adopted to distinguish *P. kugleri* from *P. pseudokugleri* are needed in order to confirm a late Oligocene occurrence of *P. kugleri*. On the contrary, we consider the Base of common *P. kugleri*, as here defined, a reliable event as it occurs just above the Top of *S. delphix* in both the Campos Basin and Hole 516F, where the *P. kugleri* Base common is associated with the lower part of Subchron C6Cn.2n in agreement with literature data. Therefore, we can consider our Base common as time-equivalent to the Base of *P. kugleri* used in the literature to approximate the O/Mb boundary (Figure 13).

Globigerinoides gr. Base and Base common occurrence – The distribution pattern of the *Globigerinoides* gr. compares well with that of the Lemme-Carrosio section (figure 3 in Iaccarino et al., 1996) and with that indicated by Spezzaferri (1992, 1994), even if we recognize both events at slightly lower stratigraphic levels, respectively. We recognize the Base of the *Globigerinoides* gr., with rare occurrences of *Globigerinoides* cf. *G. subquadratus* and *G. quadrilobatus* (making it equivalent to the *Globigerinoides* event of Spezzaferri, 1994), in the late Oligocene, even if within

Subchron C7n.2n and not Chron C6Cr, approximating the Base of *P. kugleri*. We identified the Base of regular occurrence of this group just below the O/Mb, within the range of *S. delphix* and not at the O/Mb like in the Lemme-Carrosio section (Iaccarino et al., 1996), where, however, the *S. delphix* range is poorly defined (see Aubry & Villa, 1996). Pending a definitive formulation of the redefinition of this genus provided by Spezzaferri et al. (2015), we observe that the Base of regular occurrence of the *Globigerinoides* gr. deserves further investigations to verify its usefulness at the OMT.

Globoturborotalita ciperensis gr. Top – Pearson and Chaisson (1997) observed that *G. ciperensis* disappears at the base of the Miocene at equatorial latitude (ODP Leg 154, Ceara Rise; Figure 13) and that *G. fariasi* and *G. anguliofficialis*, here comprised in the same group occur only throughout the range of *G. ciperensis*. However, we only note an overall reduction of this group (paracme interval or abundance drop) largely predating the O/Mb, within Chron C7n, followed by rare occurrences in the Campos Basin and an abundance recovery in Hole 516F (PE) in the early Miocene, at the base of Subchron C6Cn.1n. The early Miocene occurrences of this group are mainly represented by *G. ciperensis*. We argue that this species is strongly dependent on local paleoceanographic conditions and therefore we suggest that its Top should not be considered as a global marker. However, the PB/AD of the *G. ciperensis* gr., not yet reported in literature and recorded between the Base of the *Globigerinoides* gr. and the Top of *S. ciperensis* within Chron C7n, is a promising biomarker for regional correlations.

Globoturborotalita angulituralis Top – Although this event was placed in the early Miocene (Figure 13) by Berggren et al. (1983) and later recalibrated by Gradstein et al. (2012), we recorded the *G. angulituralis* Top in the late Oligocene in Well A and Hole 516F at two stratigraphic positions. Therefore, we agree with Spezzaferri (1994) that the Top of this species is not a synchronous event even at a regional scale, probably due to its scattered occurrence toward the end of its range in the late Oligocene.

Sphenolithus conicus acme interval – In the Campos Basin, *S. conicus* shows an acme interval that is comparable to that reported at Site 1218 in the Equatorial Pacific Ocean (Figure 13) by Blair (2011), showing an age range from 23.57 to 22.87 Ma and bracketing the *S. delphix* range. A similar distribution is also detectable at the middle latitude of the North Atlantic Site 563 (Maiorano & Monechi, 1998), where, differently, *S. conicus* also shows abundance peaks in the early Miocene, above the acme interval. Conversely, in the Indian Ocean Hole 710A, an acme interval is identified above the *S. delphix* range (Fornaciari et al., 1990). These observations and the absence of *S. conicus* in Hole 516F suggest that the presence of a well-defined acme relies on particular paleoceanographic conditions and its potential for global correlations is low.

Sphenolithus disbelemnus (<4 μm) range – We point out that in the Campos Basin, the smaller *S. disbelemnus* morphotype shows a different and wider stratigraphic range with respect to

S. disbelemnus, spanning from the late Oligocene, where it is approximated by the *S. delphix* Base, to the early Miocene. We thus suggest the potential value of *S. disbelemnus* <4 μm as a biostratigraphic marker. However, these small morphotypes are absent in Hole 516F, a succession depleted of sphenoliths.

Globoquadrina dehisces Base – In our material, the Base of *G. dehisces* consistently occurs between the *S. capricornutus* Top (or the Bc of *P. kugleri*) and the Base of *S. disbelemnus*. In Hole 516F, the *G. dehisces* Base is associated with Subchron C6Cn.1n, a slightly younger position than that reported by Wade et al. (2011) and Gradstein et al. (2012; Figure 13). In Hole 516F, Spezzaferri (1992) observed a peculiar distribution of this taxon, characterized by occurrences in the late Oligocene, below Chron C7An (Core 13, 284 mbsf), followed by a paracme, which ends at a level coincident with the Base identified in our work. However, our samples are stratigraphically above the occurrence described at 284 mbsf. Spezzaferri (1994) also observed such early occurrences at different levels in the late Oligocene (Zone P22) in other DSDP sites (Pacific, Southern Atlantic, and Indian Oceans), whereas in the Northern Atlantic and the Mediterranean she identified this event in the early Miocene (Zone N4). We agree that this datum is reliable only in regional settings.

Discoaster druggii Base – According to Fornaciari (1996), this event occurs in the Indian Ocean just above the *S. delphix* Top; similarly, in the Mediterranean, the *Discoaster druggii* Base was observed between the Top of *S. delphix* and the Base of *S. disbelemnus* (Fornaciari & Rio, 1996) and was therefore associated by interpolation with Subchron C6Cn.1r (Gradstein et al., 2012; Figure 13). At Site 1218 (equatorial Pacific, Pälke et al., 2006) and Site 563 (North Atlantic, Maiorano & Monechi, 1998), this event was directly correlated to the lower part of Chron C6Br (Figure 13). In our material, this taxon is only identified in Hole 516F, where it is rare and its Base is tied to the upper part of Chron C6Br, indicating a delayed position in this sector of the SW Atlantic Ocean with respect to all the above-mentioned occurrences. Therefore, we support the observation by Backman et al. (2012) that this event is globally diachronous.

Sphenolithus disbelemnus $\geq 4 \mu\text{m}$ Base – In our material, the B of *S. disbelemnus* $>4 \mu\text{m}$ occurs between the Base of *G. dehisces* (see above) and the Base of *S. cometa*, in the basal part of Subchron C6Bn.2n in Hole 516F. However, a progressively older age is indicated in the Pacific Ocean (basal part of Chron C6Br) and in the North and SE Atlantic (close to the C6Cn.1r/C6Cn.1n reversal; Figure 13). Thus, noting the regional value of this event, we suggest considering the B of *S. disbelemnus* $>4 \mu\text{m}$ globally diachronous.

Sphenolithus procerus Base – This event is only present in the Campos Basin between the Bases of *S. disbelemnus* and of *S. cometa*, which are both present in Hole 516F, allowing the projection of the *S. procerus* Base in Subchron C6Bn.2n. As this event was only reported at Site 563 within Chron C6AAr (Figure 13; Maiorano & Monechi, 1998), it is considered diachronous in the Atlantic Ocean.

Sphenolithus cometa Base – This event occurs above the Base of *S. disbelemnus* >4 μm both in the Campos Basin and in Hole 516F, where it is associated with Subchron C6Bn.2n, confirming the results obtained at Site 563 (Figure 13; Maiorano & Monechi, 1998) and reinforcing the reliability of the *S. cometa* Base as a marker within Zone NN2, at least in the Atlantic Ocean.

7 | CONCLUSION

In this work, we present a high-resolution integrated study on the basis of quantitative calcareous plankton biostratigraphy and magnetostratigraphy at the OMT. Accordingly, the biostratigraphic resolution for this interval is remarkably increased by using additional bioevents, other than those commonly used in the standard biozonations. The calcareous nannofossil events Top of *S. ciperoensis*, the Base and Top of *S. delphix*, and the Base of *S. cometa* provide the most solid contribution to the biostratigraphic framework, being present both in the Campos Basin and in the Rio Grande Rise (Hole 516F) and confirming their reliability as global markers. The O/Mb, identified at the base of Subchron C6Cn.2n in Hole 516F, is best approximated by the Top of *S. delphix*, which has been recognized despite the scarcity of sphenoliths at this site and by the Base of common *P. kugleri*, which in the SW Atlantic Ocean equates to the Base reported in the GSSP section and low-latitude open ocean. Compared to literature data, we observe that the *G. angulituralis* Top and *S. procerus* Base may change their stratigraphic position depending on their geographic distribution and are thus considered slightly diachronous at a global scale, as well as the Bases of *G. dehiscens* and *S. disbelemnus* >4 μm , which, however, are at least reliable in the SW Atlantic Ocean. The *G. ciperoensis* AD/PB, the *S. conicus* acme interval, and the *S. cometa* Base, which are seldom used in literature, proved useful to correlate the Campos Basin to the Rio Grande Rise and deserve more attention to evaluate their potential value as global markers. Our study also highlights other previously unreported bioevents only observed in the Campos Basin (the distribution range of *S. disbelemnus* <4 μm and of *Sphenolithus* cf. *S. pseudoheteromorphus*, the acme interval of *T. praestainforthi*, and the Top of common *G. primordius*), which usefully concur to integrate the standard OMT biostratigraphy.

ACKNOWLEDGEMENTS

We thank the IODP for providing access to the studied cores. The IODP is sponsored by the U.S. National Science Foundation (NSF) and participating countries under the management of Joint Oceanographic Institutions, Inc.

The authors acknowledge Petrobras (Petróleo Brasileiro SA) for financial support and for supplying samples. We are also grateful to O. Strohschoen and S. Shimabukuro (CENPES/Petrobras) for their comments that contributed to the improvement of the manuscript. Giovanna Gianelli and Luca Barchi are thanked for processing the micropaleontological samples and for the foraminiferal SEM images, respectively. Finally, we thank Walter Hale at the IODP Bremen Core Repository (BCR) for his valuable help during the sampling.

REFERENCES

- Abreu, V. S., & Haddad, G. A. (1998). Glacioeustatic fluctuations: The mechanism linking stable isotope events and sequence stratigraphy from the early Oligocene to middle Miocene. *Mesozoic and Cenozoic Sequence Stratigraphy of European basins*, SEPM Special Publication, 60, 245–259.
- Agnini, C., Fornaciari, E., Raffi, I., Catanzariti, R., Pälike, H., Backman, J., & Rio, D. (2014). Biozonation and biochronology of Paleogene calcareous nannofossils from low and middle latitudes. *Newsletters on Stratigraphy*, 47, 131–181.
- Aubry, M. P., & Villa, G. (1996). Calcareous nannofossil stratigraphy of the Lemme-Carrosio Paleogene-Neogene Global Stratotype Section and Point (NW Italy). *Giornale di Geologia*, 58, 51–69.
- Backman, J., & Raffi, I. (1997). Calibration of Miocene nannofossil events to orbitally tuned cyclostratigraphy from Ceara Rise. In N. J. Shackleton, W. B. Curry, C. Richter, & T. J. Bralower (Eds.), *Proceedings of the ODP (Scientific Results)* (pp. 83–99). College Station, TX: Ocean Drilling Program 154.
- Backman, J., Raffi, I., Rio, D., Fornaciari, E., & Pälike, H. (2012). Biozonation and biochronology of Miocene through Pleistocene calcareous nannofossils from low and middle latitudes. *Newsletters on Stratigraphy*, 45, 221–244.
- Barker, P. F., Johnson, D. A., Carlson, R. L., Čepek, P., Coulbourn, W. T., Gamboa, L. A., ... Walton, W. H. (1983). Shipboard Scientific Party: Site 516: Rio Grande Rise. In P. F. Barker, R. L. Carlson, D. A. Johnson, et al. (Eds.), *Initial Reports of the DSDP* (pp. 155–338). Washington, D.C., U.S.: Government Printing Office 72.
- Berggren, W. A., Aubry, M.-P., & Hamilton, N. (1983). Neogene magnetobiostratigraphy of Deep Sea Drilling Project Site 516 (Rio Grande Rise, South Atlantic). In P. F. Barker, R. L. Carlson, D. A. Johnson, et al. (Eds.), *Initial reports of the DSDP* (pp. 675–713). Washington, D.C., U.S.: Government Printing Office 73.
- Berggren, W. A., Kent, D. V., Swisher, C. C., & Aubry, M. P. (1995). A revised Cenozoic geochronology and chronostratigraphy. *Geochronology Time Scales and Global Stratigraphic Correlation*, SEPM Special Publication, 54, 129–212.
- Berggren, W. A., Kent, D. V., & van Couvering, J. A. (1985). The Neogene: Part 2 Neogene geochronology and chronostratigraphy. *Geological Society, London, Memoirs*, 10, 211–260.
- Berggren, W. A., & Pearson, P. N. (2005). A revised tropical to subtropical Paleogene planktonic foraminiferal zonation. *Journal of Foraminiferal Research*, 35, 279–298.
- Billups, K., Pälike, H., Channel, J. E. T., Zachos, J. C., & Shackleton, N. J. (2004). Astronomic calibration of the late Oligocene through early Miocene geomagnetic polarity time scale. *Earth and Planetary Science Letters*, 224, 33–44.
- Blair, S. A. (2011). Calcareous nannofossil biostratigraphy, evolution, and taxonomy in two problematic intervals: The Oligocene (ODP Leg 199) and Turonian (ODP leg 207). PhD Thesis, The Florida State University.
- Blair S., & Wise S. W. (2010). Astronomical calibration of calcareous nannofossil events and paleoceanographic significance across the Oligocene /Miocene boundary: ODP Leg 199, Site 1218 (eastern equatorial Pacific). *INA 13, 5-10 September 2010*, Yamagata, Japan.
- Blaj, T., Backman, J., & Raffi, I. (2009). Late Eocene to Oligocene preservation history and biochronology of calcareous nannofossils from paleo-equatorial Pacific Ocean sediments. *Rivista Italiana di Paleontologia e Stratigrafia*, 115, 67–85.
- Blow, W. H. (1969). Late middle Eocene to Recent planktonic foraminiferal biostratigraphy. 1967. In P. Bronniman, & R. R. Renz (Eds.), *Geneva, 1Proceeding first international conference planktonic microfossils* (pp. 199–422). Leiden: E.J. Brill.
- Blow, W. H., & Banner, F. T. (1962). The mid-Tertiary (upper Eocene to Aquitanian) Globigerinacea. In F. F. Eames, et al. (Eds.), *Fundamentals of mid-Tertiary stratigraphical correlation* (pp. 61–151). UK: Cambridge University Press.

- Bolli, H. M. (1957). Planktonic foraminifera from the Oligocene-Miocene Cipero and Lengua Formations of Trinidad, B.W.I. *U.S. National Museum Bulletin*, 215, 97–123.
- Bolli, H. M., & Saunders, J. B. (1985). Oligocene to Holocene low latitude planktic foraminifera, 1985. In Bolli, et al. (Eds.), *Plankton stratigraphy* (pp. 155–262). Cambridge, UK: Cambridge University Press 1–554.
- Bramlette, M. N., & Wilcoxon, J. A. (1967). Middle Tertiary calcareous nannoplankton of the Cipero section, Trinidad, W.I. *Tulane Studies in Geology and Paleontology*, 5, 93–131.
- Bukry, D. (1969). Upper Cretaceous coccoliths from Texas and Europe. *The University of Kansas Paleontological Contributions*, 51(Protista 2), 1–79.
- Cande, S. C., & Kent, D. V. (1995). Revised calibration of the geomagnetic polarity timescale for the late Cretaceous and Cenozoic. *Journal of Geophysical Research*, 100, 6093–6095.
- Curry, W. B., Shackleton, N. J., Richter, C., Backman, J. E., Bassinot, F., Bickert, T., ... Zachos, J. C. (1995). *Proceedings of the ODP*, Initial Reports 154. College Station, TX: Ocean Drilling Program.
- de Kaenel, E., & Villa, G. (1996). Oligocene-Miocene calcareous nannofossils biostratigraphy and paleoecology from the Iberia Abyssal Plain. In R. B. Whitmarsh, D. S. Sawyer, A. Klaus, & D. G. Masson (Eds.), *Proceedings of the ODP* (Initial Reports 149) (pp. 79–145). College Station, TX: Ocean Drilling Program.
- de Kaenel, E., Villa, G. (2010). Nannofossil definition of the Oligocene/Miocene boundary at Lemme-Carrosio stratotype (Italy). *INA* 13, 5–10 September 2010, Yamagata, Japan, 33.
- Ellis, C. H. (1975). Calcareous nannofossil biostratigraphy—LEG 31, DSDP. In D. E. Karig, & J. C. Ingle, Jr. (Eds.), *Initial reports of the Deep Sea Drilling Project 31* (pp. 655–676). Washington: U.S. Government Printing Office.
- Florindo, F., Gennari, R., Persico, D., Turco, E., Villa, G., Pontus, C. L., ... Pekar, S. F. (2015). New magnetobiostratigraphic chronology and paleoceanographic changes across the Oligocene-Miocene boundary at DSDP Site 516 (Rio Grande Rise, SW Atlantic). *Paleoceanography*, 30, 659–681.
- Fornaciari, E. (1996). *Biocronologia a nannofossili calcarei e stratigrafia ad eventi nel Miocene Italiano*. Ph.D Thesis, Università degli studi di Padova.
- Fornaciari, E., & Agnini, C. (2009). Taxonomic note: *Sphenolithus pseudoheteromorphus*, a new Miocene calcareous nannofossil species from the equatorial Indian Ocean. *Journal of Nannoplankton Research*, 30, 97–101.
- Fornaciari, E., Raffi, I., Rio, D., Villa, G., Backman, J., & Olafsson, G. (1990). Quantitative distribution patterns of Oligocene and Miocene calcareous nannofossils from the western equatorial Indian Ocean. In R. A. Duncan, J. Backman, L. C. Peterson, et al. (Eds.), *Proceedings of the ODP* (Scientific Results 115) (pp. 237–254). College Station, TX: Ocean Drilling Program.
- Fornaciari, E., & Rio, D. (1996). Latest Oligocene to early middle Miocene quantitative calcareous nannofossil biostratigraphy in the Mediterranean region. *Micropaleontology*, 42, 1–36.
- Gradstein, F. M., Ogg, J. G., Schmitz, M., & Ogg, G. (2012). *The geologic time scale 2012*. Amsterdam: Elsevier.
- Henderiks, J., & Pagani, M. (2007). Coccolithophore cell size and the Paleogene decline in atmospheric CO₂. *Earth and Planetary Science Letters*, 269, 576–584.
- Iaccarino, S., Borsetti, A. M., & Rogl, F. (1996). Planktonic foraminifera of the Neogene Lemme-Carrosio GSSP section (Piedmont, Northern Italy). *Giornale di Geologia*, 58, 35–49.
- Keller, G. (1981). The genus *Globorotalia* in the early Miocene of the equatorial and northwestern Pacific. *Journal of Foraminiferal Research*, 11, 118–132.
- Kennett, J. P., & Srinivasan, M. S. (1983). *Neogene planktonic foraminifera: A phylogenetic atlas: Stroudsburg* (pp. 265). Pennsylvania: Hutchinson and Ross.
- Kirschvink, J. L. (1980). The least-squares line and plane and the analysis of palaeomagnetic data. *Geophysical Journal of the Royal Astronomical Society*, 62, 699–718.
- Leckie, M. R., Farnham, C., & Schmidt, M. G. (1993). Oligocene planktonic foraminifer biostratigraphy of Hole 803D (Ontong Java Plateau) and Hole 628A (Little Bahama Bank) and comparison with the southern high latitude. In W. H. Berger, L. W. Kroenke, L. A. Mayer, et al. (Eds.), *Proceedings of the ODP* (Scientific Results 130) (pp. 113–136). College Station, TX: Ocean Drilling Program.
- Li, Q., Jian, Z., & Li, B. (2004). Oligocene–Miocene planktonic foraminifer biostratigraphy, Site 1148, northern South China Sea. In W. L. Prell, P. Wang, P. Blum, et al. (Eds.), *Proceedings of the ODP* (Scientific Results 184) (pp. 1–26). TX (Ocean Drilling Program): College Station.
- Liebrand, D., Beddow, H. M., Lourens, L. J., Pälike, H., Raffi, I., Bohaty, S. M., ... Batenburg, S. J. (2016). Cyclostratigraphy and eccentricity tuning of the early Oligocene through early Miocene (30.1–17.1Ma): *Cibicides mundulus* stable oxygen and carbon isotope records from Walvis Ridge Site 1264. *Earth and Planetary Science Letters*, 450, 392–405.
- Lourens, L., Hilgen, F., Shackleton, L., & Wilson, J. D. (2004). The Neogene period. In F. M. Gradstein, J. G. Ogg, & A. Smith (Eds.), *A geologic time scale 2004* (pp. 409–440). Cambridge, UK: Cambridge University Press.
- Lurcock, P. C., & Wilson, G. S. (2012). PuffinPlot: A versatile, user-friendly program for paleomagnetic analysis. *Geochemistry, Geophysics, Geosystems*, 13, Q06Z45, <https://doi.org/10.1029/2012GC004098>.
- Lyle, M. W., Wilson, P. A., Janecek, T. R., Backman, J., Busch, W. H., Coxall, H.K., ... Wade, B. (2002). Site 1218. In: *Proceedings of the Ocean Drilling Program, Initial reports, Paleogene equatorial transect; covering Leg 199 of the cruises of the drilling vessel JOIDES Resolution; Honolulu, Hawaii, to Honolulu, Hawaii; sites 1215-1222; 23 October-16 December 2001*.
- Maiorano, P., & Monechi, S. (1998). Revised correlation of early and middle Miocene calcareous nannofossil events and magnetostratigraphy from DSDP Site 563 (North Atlantic Ocean). *Marine Micropaleontology*, 35, 235–255.
- Martini, E. (1971). Standard tertiary and quaternary Calcareous nannoplankton zonation. In Farinacci (Ed.), *Proceedings of the II planktonic conference* (pp. 739–785). Roma: Tecnoscienza 2.
- Miller, K. G., Aubry, M. P., Khan, M. J., Melillo, A. J., Kent, D. V., & Berggren, W. A. (1985). Oligocene-Miocene biostratigraphy, magnetostratigraphy, and isotopic stratigraphy of the Western North Atlantic. *Geology*, 13, 257–261.
- Mohriak, W. U., Mello, M. R., Dewey, J. F., & Maxwell, J. R. (1990). Petroleum geology of the Campos Basin, offshore Brazil. *Geological Society, London, Special Publications*, 50, 119–141.
- Okada, H., & Bukry, D. (1980). Supplementary modification and introduction of code numbers to the low-latitude coccolith biostratigraphic zonation (Bukry, 1973; 1975). *Marine Micropaleontology*, 5, 321–325.
- Olsson, R. K., Pearson, P. N., & Huber, B. T. (2006). Taxonomy, biostratigraphy, and phylogeny of Eocene *Catapsydrax*, *Globorotaloides*, *Guembeltrioides*, *Paragloborotalia*, *Parasubbotina*, and *Pseudoglobigerinella* n. gen. In P. N. Pearson, et al. (Eds.), *Atlas of Eocene Planktic Foraminifera* (pp. 67–110). Washington, DC: Cushman Foundation for Foraminiferal Research, Special Publication 41.
- Pagani, M., Arthur, M. A., & Freeman, K. (2000). Variations in Miocene phytoplankton growth rates in the Southwest Atlantic: Evidence for changes in ocean circulation. *Paleoceanography*, 15, 486–496.
- Pälike, H., Frazier, J., & Zachos, J. C. (2006). Extended orbitally forced palaeoclimatic records from the equatorial Atlantic Ceara Rise. *Quaternary Science Reviews*, 25, 3138–3149.
- Pälike, H., Moore, T., Backman, J., Raffi, I., Lanci, L., Parés, J. M., & Janecek, T. (2005). Integrated stratigraphic correlation and improved composite depth scales for ODP Sites 1218 and 1219. In P. A. Wilson, M. Lyle, & J. V. Firth (Eds.), *Proceedings of the ODP* (Scientific Results 199) (pp. 1–41). Ocean Drilling Program: College Station, TX.
- Pearson, P. N. (1995). Planktonic foraminifer biostratigraphy and the development of pelagic caps on guyots in the Marshall Islands group. In J. A. Haggerty, I. Premoli Silva, F. Rack, & M. K. McNutt (Eds.), *Proceedings of*

- the Ocean Drilling Program (Scientific Results 144) (pp. 21–59). Ocean Drilling Program: College Station, TX.
- Pearson, P. N., & Chaisson, W. P. (1997). Late Paleocene to middle Miocene planktonic foraminifer biostratigraphy of the Ceara Rise. In N. J. Shackleton, W. B. Curry, C. Richter, & T. J. Bralower (Eds.), *Proceedings of the ODP (Scientific Results 154)* (pp. 33–68). Ocean Drilling Program: College Station, TX.
- Pearson, P. N., & Wade, B. S. (2009). Taxonomy and stable isotope paleoecology of well-preserved planktonic foraminifera from the uppermost Oligocene of Trinidad. *Journal of Foraminiferal Research*, 39, 191–217.
- Planca, J., Grossi, V., Henderiks, J., Simon, L., & Mattioli, E. (2012). Alkenone producers during late Oligocene-early Miocene revisited. *Paleoceanography*, 27, PA1202.
- Planca, J., Mattioli, E., Henderiks, J., & Grossi, V. (2013). Global shifts in Noelaerhabdaceae assemblages during the late Oligocene-early Miocene. *Marine Micropaleontology*, 103, 40–50.
- Pujol, C. (1983). Cenozoic planktonic foraminiferal biostratigraphy of the Southwestern Atlantic (Rio Grande Rise): Deep Sea Drilling Project Leg 72. In P. E. Barker, R. L. Carlson, D. A. Johnson, et al. (Eds.), *Initial reports of the DSDP 72* (pp. 623–673). Washington: U.S. Govt. Printing Office.
- Raffi, I., Backman, J., Fornaciari, E., Pälike, H., Rio, D., Lourens, L., & Hilgen, F. J. (2006). A review of calcareous nannofossil astrobiochronology encompassing the past 25 million years. *Quaternary Science Reviews*, 25, 3113–3137.
- Rio, D., Fornaciari, E., & Raffi, I. (1990). Late Oligocene through early Pleistocene calcareous nannofossils from western equatorial Indian Ocean (Leg 115). In R. A. Duncan, J. Backman, L. C. Peterson, et al. (Eds.), *Proceedings of the ODP (Scientific Results 115)* (pp. 175–235). College Station, TX: Ocean Drilling Program.
- Shackleton, N. J., Hall, M. A., Raffi, I., Tauxe, L., & Zachos, J. (2000). Astronomical calibration age for the Oligocene-Miocene boundary. *Geology*, 28, 447–450.
- Spezzaferri, S. (1991). Evolution and taxonomy of the *Paragloborotalia kugleri* (Bolli) lineage. *Journal of Foraminiferal Research*, 21, 313–318.
- Spezzaferri, S. (1992). The Oligocene/Miocene boundary in the “Oceanic record” (Atlantic, Indian and Pacific Ocean): Biostratigraphy and paleoclimatology. *Paléo*, 2, 79–88.
- Spezzaferri, S. (1994). Planktonic foraminiferal biostratigraphy of the Oligocene and lower Miocene in the oceanic record. An overview. *Palaeontographia Italica*, 81, 1–187.
- Spezzaferri, S. (1996). Paleoclimatic interpretation of the late Oligocene-early Miocene planktonic foraminiferal record from the Lemme-Carrosio section (northern Italy). *Giornale di Geologia*, 58, 119–139.
- Spezzaferri, S., Kucera, M., Pearson, P. N., Wade, S. W., Rappo, S., Poole, C. R., ... Stadler, C. (2015). Fossil and genetic evidence for the polyphyletic nature of the planktonic foraminifera “Globigerinoides”, and description of the new genus *Trilobatus*. *PLoS One*, 10.
- Stainforth, R. M., Lamb, J. L., Luterbacher, H., Beard, J. H., & Jeffords, R. M. (1975). Cenozoic planktonic foraminiferal zonation and characteristics of index forms. *Paleontological Contributions*, 62, 425.
- Steininger, F. F., Aubry, M. P., Berggren, W. A., Beard, J. H., & Jeffords, R. M. (1997). The Global Stratotype Section and Point (GSSP) for the base of the Neogene. *Episodes*, 20, 23–28.
- Steininger, F., & Iaccarino, S. M. (1996). Synthesis on the GSSP Lemme-Carrosio section. *Giornale di Geologia*, 58, 141–147.
- Wade, B. S., Pearson, P. N., Berggren, W. A., & Pälike, H. (2011). Review and revision of Cenozoic tropical planktonic foraminiferal biostratigraphy and calibration to the geomagnetic polarity and astronomical time scale. *Earth Science Reviews*, 104, 111–142.
- Wei, W., & Wise, S. W. Jr. (1989). Paleogene calcareous nannofossil magnetobiochronology: Results from South Atlantic DSDP Site 516. *Marine Micropaleontology*, 14, 119–152.
- Zijderveld, J. D. A. (1967). A. C. demagnetization of rocks: Analysis of results. In D. W. Collinson, K. M. Creer, & S. K. Runcorn (Eds.), *Methods in palaeomagnetism* (pp. 254–286). Amsterdam: Elsevier, Developments in Solid Earth Geophysics, 3.

SUPPORTING INFORMATION

Additional Supporting Information may be found online in the supporting information tab for this article.

How to cite this article: Gennari R, Persico D, Turco E, et al. High-resolution integrated calcareous plankton biostratigraphy and magnetostratigraphy at the Oligocene–Miocene transition in Southwestern Atlantic Ocean. *Geological Journal*. 2018;53:1079–1101. <https://doi.org/10.1002/gj.2945>

APPENDIX

TAXONOMIC REMARKS OF SELECTED PLANKTONIC FORAMINIFERA

The *Paragloborotalia pseudokugleri*–*P. kugleri* lineage

This lineage represents an important taxonomic group at the OMT. Stainforth, Lamb, Luterbacher, Beard, and Jeffords (1975), Kennett and Srinivasan (1983) and Bolli and Saunders (1985) considered the differences between *P. kugleri* (Bolli, 1957) and *P. pseudokugleri* (Blow, 1969) relatively minor and thus unnecessary to separate them. On the other hand, the majority of the authors (e.g., Keller, 1981; Berggren et al., 1983, 1985, 1995; Spezzaferri, 1991, 1994; Leckie et al., 1993; Pearson, 1995; Iaccarino et al., 1996; Steininger & Iaccarino, 1996; Lyle et al., 2002; Li, Jian, & Li, 2004; Berggren & Pearson, 2005; Pearson & Wade, 2009) distinguish these taxa, considering *P. pseudokugleri* as the ancestral form

of *P. kugleri* (following Blow, 1969) and recognize their great stratigraphic importance at the Oligocene–Miocene transition. In fact, the Base of *P. kugleri* defines the lower boundary of Zone M1 (Berggren et al., 1995; Wade et al., 2011) and is used to approximate the O/Mb (Berggren et al., 1983, 1985, 1995; Steininger et al., 1997).

For this reason and because of the gradual morphological transition between *P. pseudokugleri* and *P. kugleri*, it is very important to have clear criteria to distinguish the two species. *P. kugleri*, which was first described by Bolli (1957, Pl. 28, 5 and 6), shows the following major features: “equatorial periphery slightly lobate, axial periphery rounded or with the tendency to become subangular, chambers ovate,... sutures on spiral side curved and depressed, 6–8 chambers in the last whorl” (see Figure 7(b), b1–b3). Bolli (1957) also illustrated a form with inflated subglobular chambers and nearly radial sutures on spiral side (*P. cf. kugleri* in Pl. 28, fig. 7; Figure 7(b), a1–a3). This form was later indicated and described as the holotype of *P. pseudokugleri* by Blow

(1969) as follows: “chambers inflated both dorsally and ventrally, test very nearly equally biconvex, but with a smoothly rounded broad, not subacute, peripheral margin,” “subglobular chambers,” and “nearly radial dorsal” sutures. According to Blow (1969), *P. pseudokugleri* differs from *P. kugleri* “in not having a flat dorsal surface to the test but in having inflated, subglobular chambers with radial dorsal intercameral sutures.” The original definition of *P. kugleri*, characterized by the curved spiral sutures and a peripheral margin rounded or with the tendency to become subangular, was successively modified by authors who limited the description of the axial profile to (a) slightly angled (Keller, 1981; Figure 7(b), d1–d3); (b) subacute and more or less biconvex (Spezzaferri, 1991, 1994; Figure 7(b), e1–e3); (c) subacute (Leckie et al., 1993; Figure 7(b), f1–f2). In addition, Spezzaferri (1991), introduced together with the biconvexity, the curved sutures also on the umbilical side as distinctive features of *P. kugleri* s.s. (Figure 7(b), e3). More recently, Pearson and Wade (2009) pointed out that in the material collected in the type locality (Cipero Formations of Trinidad) the population of *P. pseudokugleri* shows quite advanced features, and assigned the specimens (illustrated in their Pl. 6, fig. 11, our Figure 7 (b), g) with “strongly curved sutures and appressed chambers but with rounded axial profile” to *P. pseudokugleri*. Therefore, the distinctive feature of *P. kugleri*, according to Pearson and Wade (2009), seems to be the subacute axial profile. Considering the different criteria adopted by the above-mentioned authors, it follows that there is no consensus on the features that characterize the axial profile of *P. kugleri*, and hence on its definition.

In this study, specimens characterized by generally six globular chambers in the last whorl, straight and nearly radial sutures on both dorsal and umbilical side, rounded margin, and a lobate profile (Figure 7(a), a1–a3), well correspond to *P. pseudokugleri* holotype of Blow (1969) (Figure 7(b), a1–a3). In Hole 516F, in correspondence of the levels of highest abundance of *P. pseudokugleri*, specimens showing ovate shape of the chambers, curved dorsal sutures, rounded to more subacute axial periphery, and poorly lobate outline (Figure 7(a), b–g) are recorded within the population of this taxon. These specimens show the morphological features distinctive of *P. kugleri* according to the original definition of Bolli (1957), and they closely resemble the *P. kugleri* specimens observed in the Base level of the Lemme-Carrosio section (Neogene GSSP) just above the O/Mb (Iaccarino et al., 1996; Figure 7(b), h1–h3), and those figured by Keller (1981; Figure 7(b), d1–d3) and Leckie et al. (1993; Figure 7(b), f1–f2). The most evolved forms according to Spezzaferri (1991, 1994; i.e., *P. kugleri* s.s., Figure 7(b), e1–e3) were not observed in the studied assemblages.

***Globigerinoides* gr.**

The *Globigerinoides* genus has been revised by Spezzaferri et al. (2015), who propose to erect a new genus (*Trilobatus*) for those forms descending from *Globigerinoides* (*Trilobatus*) *primordius* (*Trilobatus*

immaturus, *Trilobatus praeimmaturus*, *T. primordius*, *Trilobatus subsacculifer*, *Trilobatus trilobus*, *Trilobatus bisphericus*, *Trilobatus sicanus*, and *Trilobatus sacculifer*). Accordingly, the genus *Globigerinoides* is emended and retained for those species phylogenetically related to the genus *Globoturbotalita* (*Globigerinoides bollii*, *Globigerinoides italicus*, *Globigerinoides obliquus*, *Globigerinoides extremus*, *Globigerinoides quadrilobatus*, *Globigerinoides subquadratus*, *Globigerinoides ruber*, *Globigerinoides bulloideus*, and *Globigerinoides elongatus*). However, for its biostratigraphic value (*Globigerinoides* event of Spezzaferri, 1994 and Iaccarino et al., 1996), we retain the *Globigerinoides* gr. and, following Iaccarino et al. (1996), we plotted under this group all the *Globigerinoides* species recognized in our material (Figure 8, b and c represent a few species included in the gr.), except for *G. primordius*.

Globigerinoides primordius

According to Blow and Banner (1962), the first *Globigerinoides* species corresponds to *Globigerinoides quadrilobatus primordius* (here *G. primordius*), which evolved from *Globigerina praebulloides occlusa* by adding a supplementary aperture on the dorsal side. Similarly, Spezzaferri (1994) noted that *G. primordius* differs from the *G. praebulloides* group (including *G. praebulloides*, *G. ouachitaensis*, and *G. officinalis*) only by adding secondary apertures. Actually, *G. praebulloides* has a smooth and spinose wall texture, whereas *G. praebulloides occlusa* and *G. ouachitaensis* were placed in the *Globoturbotalita* genus (Olsson, Pearson, & Huber, 2006), showing a cancellate, perforate, and spinose wall texture. Because of its *bulloides*-type wall, Pearson and Wade (2009) included *primordius* in the “*Globigerina*” genera, although they noticed that the wall might appear cancellate in places (see Pl. 4, 3d and 3e in Pearson & Wade, 2009). In our assemblages as well, we included in *G. primordius* those specimens morphologically similar to *G. praebulloides*, with a secondary aperture on the spiral side, but also those that show transitional morphologies between *G. primordius* and *G. quadrilobatus* (prevalently observed in the Petrobras wells). In contrast to *G. praebulloides*, *G. primordius* shows different types of wall structures: cancellate, perforate, and spinose (Figure 8, h1–h3) and/or smooth and spinose. These two types of structure can coexist in the same specimen and this is particularly evident in Hole 516F, due to the better preservation of the planktonic foraminiferal assemblages (Figure 8, i1–i3). In this case, the smooth and spinose wall is typical of the last chamber (Figure 8, i4) while the development of the typical polygonal pattern of the cancellate structure can be observed in the earlier chambers (Figure 8, i5). Recently, Spezzaferri et al. (2015) proposed to include *G. primordius* into the new genus *Trilobatus*, differently from *G. quadrilobatus*; however, as we observed transitional characters between the two species, we prefer to retain the old taxonomy, pending further observations on these two species.